AGU ADVANCING EARTH AND SPACE SCIENCE

Water Resources Research®

RESEARCH ARTICLE
10.1029/2021WR029679

Key Points:

- Laboratory and numerical simulations of brine leakage were used in lieu of field studies to explore source condition uncertainty impacts
- Uncertainty in storage formation's permeability field and leakage source can cause significant errors in predicted brine plume
- Defining the hydro-structural settings of caprock fractures is important for the model to predict the brine plume accurately

Supporting Information:

Supporting Information may be found in the online version of this article.

Correspondence to:

A. H. Askar,
ahmedaskar6@gmail.com

Citation:

Askar, A. H., Illangasekare, T. H., Trautz, A., Solovský, J., Zhang, Y., & Fučík, R. (2021). Exploring the impacts of source condition uncertainties on far-field brine leakage plume predictions in geologic storage of CO_2: Integrating intermediate-scale laboratory testing with numerical modeling. *Water Resources Research*, *57*, e2021WR029679. https://doi.org/10.1029/2021WR029679

Received 2 FEB 2021
Accepted 21 AUG 2021

Exploring the Impacts of Source Condition Uncertainties on Far-Field Brine Leakage Plume Predictions in Geologic Storage of CO_2: Integrating Intermediate-Scale Laboratory Testing With Numerical Modeling

Ahmad H. Askar[1], Tissa H. Illangasekare[1], Andrew Trautz[1,3], Jakub Solovský[2], Ye Zhang[4], and Radek Fučík[2]

[1]Center for Experimental Study of Subsurface Environmental Processes, Department of Civil and Environmental Engineering, Colorado School of Mines, Golden, CO, USA, [2]Department of Mathematics, Faculty of Nuclear Sciences and Physical Engineering, Czech Technical University in Prague, Prague, Czech Republic, [3]U.S. Army Corps of Engineers Engineering Research and Development Center, Geotechnical and Structures Laboratory, Vicksburg, MS, USA, [4]Geology and Geophysics Department, University of Wyoming, Laramie, WY, USA

Abstract Natural fissures/faults or pressure-induced fractures in the caprock confining injected CO_2 have been identified as a potential leakage pathways of far-field native brine contaminating underground sources of drinking water. Developing models to simulate brine propagation through the overlaying formations and aquifers is essential to conduct reliable pre- and post-risk assessments for site selection and operation, respectively. One of the primary challenges of performing such simulations is lack of adequate information about source conditions, such as hydro-structural properties of caprock fracture/fault zone and the permeability field of the storage formation. This research investigates the impact of source condition uncertainties on the accuracy of leaking brine plume predictions. Prediction models should be able to simulate brine leakage and transport in complex multilayered geologic systems with interacting regional natural and leakage flows. As field datasets are not readily available for model testing and validation, three comprehensive intermediate-scale laboratory experiments were used to generate high-resolution spatiotemporal data on brine plume development under different leakage scenarios. Experimental data were used to validate a flow and transport model developed using existing code FEFLOW to simulate brine plume under varying source conditions. Spatial moment analysis was conducted to evaluate how uncertainty in source conditions impacts brine migration predictions. Results showed that inaccurately prescribing the permeability field of storage formation and caprock fractures in models can cause errors in leakage pathway and spread predictions up to ~19% and ~100%, respectively. These findings will help in selecting and characterizing storage sites by factoring in potential risks to shallow groundwater resources.

Plain Language Summary Storing anthropogenically emitted CO_2 gas in deep saline formations is being evaluated as a strategy to reduce greenhouse gas concentrations in the atmosphere. Potential pathways, such as natural fissures or cracks induced during high-pressure injection within the confining caprock of a storage formation can result in the leakage of formation fluids into shallow aquifers used for potable water. Technical and cost constraints limit collecting high-resolution spatial and temporal data to fully define the leakage source conditions and validate the numerical models of brine migration. Different factors contribute to source uncertainties making numerical prediction of the leaking brine migration challenging. We explored the impacts of incomplete information about leakage source on the model prediction of plume development. As detailed field data are not readily available for validating numerical models for this application, data was generated in a laboratory test tank. Results showed that errors in the estimates of storage formation permeability field and caprock fractures can lead to considerable deviations in the location of predicted far-field brine plume. This study provides insight into the importance of considering inherent uncertainties in leakage source conditions for shallow aquifer contamination risk assessment. Stakeholders can use the study findings to evaluate such risk assessment reliability.

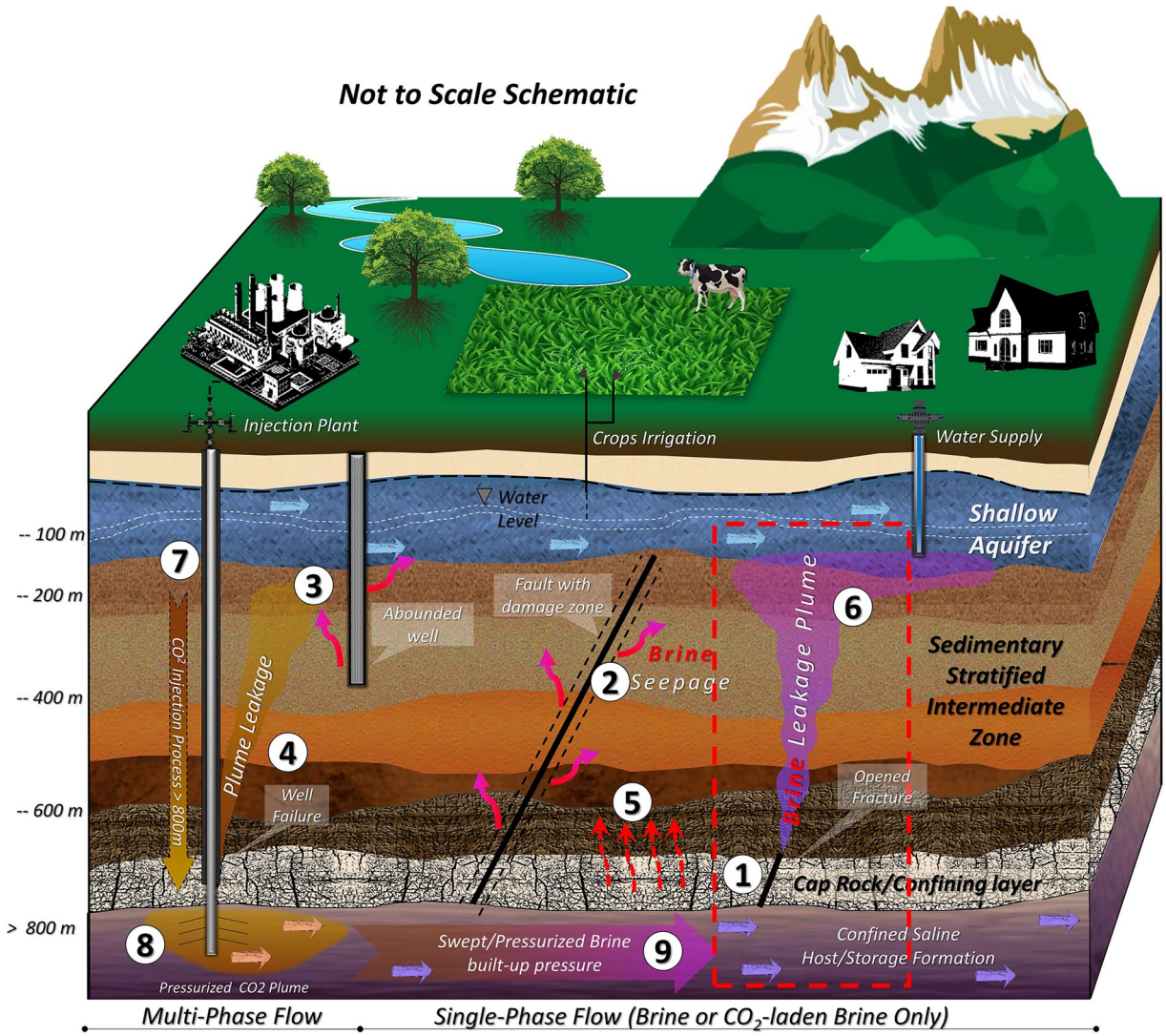

Figure 1. Conceptual model depicting potential deep brine leakage pathways as a consequence of CO_2 sequestration. Numbers correspond to (1) natural fractures, (2) fault damage zone, (3) abandoned deep wells, (4) cement failure in the injection well, (5) brine diffusion, (6) brine leakage plume, (7) injection well (*CO_2/liquid waste/HF fluids*), (8) injected CO_2/liquid waste plume, (9) displaced brine (Li & Liu, 2016; Nelson et al., 2005; Pan et al., 2013). Dashed red line represents the spatial scope of this study (i.e., far-field brine leakage).

1. Introduction

CO_2 geological sequestration (CGS) is a promising technique, that is, being applied to alleviate the atmospheric loading of greenhouse gases contributing to global warming. Deep saline formations are identified as an efficient potential repositories for captured CO_2 due to their high storage capacity and availability around the world (Bachu, 2003; Intergovernmental Panel on Climate Change, 2005; Lackner, 2003; U.S. DOE, 2015). The pressure buildup associated with CO_2 injection is shown to displace native brines within the storage formation over significant spatial areas (Birkholzer et al., 2011; Birkholzer & Zhou, 2009; Cavanagh & Wildgust, 2011; Nicot, 2008; Van der Meer, 1992). Natural discontinuities (i.e., faults, fractures, etc.), pressure-induced pathways (i.e., activated faults and new fractures), and/or local abandoned deep wells within the local and regional storage formation caprock can act as a leakage pathways from which far-field native brine can escape (Figure 1; Celia et al., 2011; Gasda et al., 2004; Rutqvist et al., 2007, 2008). In the occurrence of brine leakage, the quality of water in overlying aquifers can be detrimentally impacted and underground sources of drinking water (USDW) can be contaminated through increased salinity, elevated TDS concentrations, and/or the introduction of toxic trace metals (such as Pb, Cd, etc.; Birkholzer

et al., 2009; Gupta & Yadav, 2020; Jones et al., 2015; Qafoku et al., 2017). Contaminating the USDWs can occur through two mechanisms; (a) the poor-quality native brine leaks upward and mixes with the potable groundwater or (b) the leaking storage-formation fluids trigger the migration of the overlying saline water affecting the shallow aquifer quality (Delfs et al., 2016; Kissinger et al., 2017; Tillner et al., 2013, 2016).

In response to the potential contamination risk of CGS operations on shallow aquifers, the US Environmental Protection Agency (EPA) established the underground injection control program to provide regulatory framework for the protection of USDWs. Under this program, a set of requirements regarding the planning and construction of CGS projects must be fulfilled to ensure the safe and efficient long-term trapping of injected CO_2 (U.S. EPA, 2010); additional CGS project risk analysis and management guidelines were released by the Department of Energy (NETL, 2017). Quantifying the risk of USDW contamination by injected CO_2 has become a key consideration at all stages of project development (Pawar et al., 2015; Sun, Zeidouni, et al., 2013). One of the goals of CGS risk assessment involves the prediction of brine leakage scenarios that allow areas that will likely be impacted to be identified and pre-leakage mitigation strategies developed (Li & Liu, 2016; Pawar et al., 2015).

Several field-scale numerical studies highlighted that the main controllers of the leakage rate from a CGS storage formation are pressure buildup magnitude, extent of spread (Birkholzer & Zhou, 2009; Lions et al., 2014; Nicot, 2008; Person et al., 2010; Yamamoto et al., 2009; Zhou et al., 2010) and the permeability of storage formation and caprock damage zones (Bricker et al., 2012; Wainwright et al., 2013; Xie, Zhang, Hu, Wang, & Chen, 2015, Xie, Zhang, Hu, Wang, Pavelic, et al., 2015; Zhao et al., 2012). Jeanne et al. (2013) and Vialle et al. (2016) found that the permeability distribution of the caprock damage zone can significantly affect the predicted CO_2 leakage pathways. Hyman et al. (2020) similarly showed that the leakage of supercritical carbon dioxide from a storage formation is sensitive to the permeability, connectivity, and structure of the caprock fracture network (i.e., fracture density); the effect of variation in the network structure was found to be stronger than that of the permeability magnitude variation. All of these studies indicate that the spatiotemporal evolution of a leaking brine is dependent on the source conditions including: (a) sizes, locations, and permeabilities of caprock fractures and (b) permeability field and boundary conditions of the CO_2 storage formation.

Identifying source conditions becomes more complicated after the commencement of the injection phase of CGS operations as the geomechanical stresses and geochemical reactions induced by CO_2 injection will continuously alter the hydraulic and structural properties of caprock fractures. Geomechanical responses of the caprock fractures can include sliding, dilating, closing, opening, and intersecting with other fractures. Such structural alteration in the caprock fractures can affect their permeability, mass transport, and dominant fluid pathways (Detwiler & Morris, 2019; Lei et al., 2017). Geochemical reactions, such as dissolution and precipitation process, can also occur if the mixture of the formation brine and injected CO_2 are not at chemical equilibrium with caprock minerals (Andreani et al., 2008; Morris et al., 2016; Rathnaweera et al., 2016; Ross et al., 1981). Therefore, after CO_2 injection the caprock damage zone turns into a dynamic system exhibiting constantly changing properties.

Characterizing leakage source conditions with the level of detail necessary to ensure the accuracy of brine leakage prediction in CGS risk assessments poses several technical and financial challenges. To evaluate the impact of source condition uncertainties a transport model validated using high-resolution data on the system hydrogeological settings and the spatiotemporal development of the brine plume is required. Due to field data paucity, Keating et al. (2010) suggested three research strategies to investigate CO_2/brine leakage related issues: (a) relying on data from the engineered and well-characterized CGS pilot sites, such as Frio or Ketzin sites (Doughty et al., 2008; Kharaka et al., 2006, 2009, 2013; Nowak et al., 2013; Zeidouni et al., 2014), (b) utilizing data from analog systems, such as leakage of re-injected produced water (Jacobs, 2009; Thamke & Craig, 1997; Thamke & Midtlyng, 2003) or natural brine leakage from deep formations (Keating et al., 2010, 2014; Keating, Hakala, et al., 2013; Keating, Newell, et al., 2013; Llewellyn, 2014), and (c) generating data under controlled laboratory experiments (Agartan, 2015; Luyun et al., 2011; Trevisan et al., 2017).

Given that the objective of engineered pilot sites is to prevent leakage to examine CO_2 trapping under field conditions and the availability of high-resolution spatiotemporal data from CGS analog sites is scarce, this study adopts a laboratory-based approach. Following the conceptual model presented in Figure 1 and dis-

cussed in the proceeding section, a series of three intermediate scale experiments were designed to obtain the needed data. A large soil tank was packed in a multi-layered configuration representing a geological system consisting of a deep storage formation, multiple intermediate layers, and a shallow aquifer. Much like a CGS site, this creates a series of hydraulically connected aquifers with complex interacting multidimensional flow fields that affect plume development and travel times. These flow fields, represented in the experiments, are controlled simultaneously by different boundary conditions, such as regional (shallow and deep) hydraulic gradients, local fracture flows, and the overall pressure perturbations associated with CO_2 injection. Since brine leakage development and migration are site-specific problems that vary with the hydraulic and geological conditions of every CO_2 storage site, these experiments were not intended to reproduce the complexity of a specific CGS site. However, the goal of the experiments was to capture some of the important processes in the field to provide a much more reasonable way to validate the model for conducting theoretical analysis, which will help understanding the leakage controls and gain useful insights on the design of CGS systems.

The experimentally generated high-resolution spatiotemporal data was then used to calibrate and validate a transport model developed using FEFLOW (Diersch, 2014) to evaluate the impact of multiple uncertainty scenarios of source conditions. The results of these numerical experiments provided new insights into the impacts of leakage source conditions on the evolution of a far-field brine plume from a storage formation as a result of CGS activities. A brine leakage signal in shallow aquifers can be used as an early warning for CO_2 leakage due to its rapid migration (Réveillère & Rohmer, 2011; Sun, Nicot, & Zhang, 2013). Designing a monitoring system to detect this leakage requires a reasonable prediction of the leakage plume pathways. The results of this study highlight also the most important source parameters that need to be accurately represented in the model to obtain reasonable prediction of the far-field brine leakage for adequately designing such monitoring systems.

2. Experimental Materials and Methods

2.1. Conceptual Model and Experimental Design

A conceptual model for far-field brine leakage from a storage formation was synthesized from a number of field studies of brine leakage in analog systems to CGS (e.g., Jacobs, 2009; Keating et al., 2010, Keating, Hakala, et al., 2013; Keating, Newell, et al., 2013, 2014; Llewellyn, 2014; Thamke & Craig, 1997; Thamke & Midtlyng, 2003). In this model, a far-field brine plume is leaking from a CO_2 storage formation (denoted as Zone 1) through fractured caprock, in turn migrating via advection and dispersion through the intermediate overburden layers (denoted as Zone 2) and eventually propagating in the shallow aquifer (denoted as Zone 3). The advective flux is driven primarily by the high pressure transmitted from the storage formation during the leakage event, which creates a vertical hydraulic gradient causing the plume upward migration with minimal density effects in the vicinity of the source. The further migration of the plume through Zone 2 will be slightly retarded because of density effects (Wunsch et al., 2013), which will become less significant with distance from the leakage source as the plume dilutes.

Natural systems display depth-dependent temperature variations, which from a modeling perspective, requires that variable-density flow be coupled with both heat flow and brine transport (Zhang et al., 2005). Following Birkholzer et al. (2011), this study assumes isothermal conditions given the opposing effects that temperature and pressure exert on the brine density at varying depths. Moreover, as the multiphase flow dynamics induced by injected CO_2 have a negligible impact on the pressure response of far-field native brine (Bandilla et al., 2015; Cihan et al., 2013), single-phase flow conditions were assumed in the study. In natural systems, flow within Zones 1 and three is relatively horizontal and controlled by local and regional gradients. Flow within Zone 2 in the vicinity of a leak is predominantly vertical as it is controlled by the overall head difference between Zones 1 and 3. For simplifying the experimental settings, natural lateral flow in Zone 2 was assumed to be relatively insignificant compared to the leakage-driven vertical flow from the caprock fractures. Henceforth in the article, far-field brine leakage will be referred to as brine leakage.

Designing an experiment for understanding fundamental processes and calibrating a flow and transport model, both used to investigate the impacts of source conditions on the leakage of brine from CO_2 storage formations, is challenging because it requires; (a) the experiment, and numerical model in turn, to be able to

capture the broad range of time and length scales of the CGS related processes as brine leakage, (b) detailed knowledge about the subsurface geological settings, source conditions, and flow fields, and (c) accurate data with high spatiotemporal resolutions on the development and migration of brine leakage for model calibration. In this study, many of these challenges were addressed through its reliance on the concept of intermediate-scale testing, which as Lenhard et al. (1995) and Oostrom et al. (2007) pointed out, can be used to reproduce filed-scale groundwater flow processes in the laboratory setting while keeping initial and boundary conditions under full control. Several researchers have conducted intermediate-scale experiments to explore various aspects of CGS (Agartan, 2015; Luyun et al., 2011; Plampin et al., 2017; Solovský et al., 2020; Trevisan et al., 2017). Intermediate-scale testing is performed in test-systems with spatial length scales that are intermediary to the traditional column-scale and field scale, allowing scale-dependent natural phenomena to be reproduced. In this project the strata in natural geologic basins and formations, 1–2 km in depth, was downscaled significantly to the order of 10 m to enable laboratory experimentation. As will be shown, the heterogeneity and layering associated with this problem can be explicitly defined using geostatistical methods. Meanwhile, the multidimensional flow fields can also be prescribed and maintained via multiple boundary conditions. By this, the natural system complexities can be reproduced with efficient imitation of the multiscale interactive processes.

Despite downscaling this CGS problem to the laboratory setting, it still offers a significant space requirement challenge. Instead of creating a large vertical soil tank to conduct this work, the authors adopted a novel approach in which a long horizontal tank was used to simulate the brine leakage problem, essentially rotating the overall scenario by 90°. The soil tank was packed in a series of vertical layers analogous to the horizontal layering of the natural sedimentary formations. An impermeable "caprock" containing fractures was located between Zones 1 and 2. A vertical flow was established at both ends of the soil tank (i.e., horizontal flow in natural system) to represent the regional/local gradients controlling horizontal groundwater flow. Horizontal flow (i.e., vertical flow in natural system) across Zone 2 was induced in the experiments by adjusting the head difference between Zone 1 and Zone 3 (Figure 2b). The native brine was assumed to be uniform throughout the storage formation and therefore no transport resulting from concentration gradients is possible. In the experiments, a dyed bromide tracer was used as a surrogate for the brine found in natural formations. The brine was injected at the downstream exit of the fractures in the caprock to simulate brine leakage. The bromide was furthermore injected at sufficiently low concentrations so as to prevent flow instabilities and plume sinking due to density variation—an important consideration given that the direction of gravity is different in the experimental setup than in the field setting. It should be noted that the terms "vertical" and "horizontal" were used throughout the article to describe the flow and system directions according to natural settings. However, the terms "longitudinal" and "transversal" were used mainly to describe the plume movement and spread with respect to the principal direction of plume migration in the tank.

2.2. Intermediate-Scale Test Tank

Experiments were performed in the soil tank shown schematically in Figure 2a. The total internal dimensions of the tank were 800 cm × 123 cm × 6.5–8.0 cm (length × height × width). Tank sections with materials presented in Figure 2a were connected via a quarter cylindrical aluminum tank, creating the L-shape depicted in Figure 2a; this was a necessary design feature given the space constraints in the laboratory. The low flow velocities (Reynold's number <1.0) ensured negligible head loss along the cylindrical portion where the flow was turned 90°. The top of the soil tank was sealed with a flat plate so as to create a no-flow boundary. The use of glass walls in the soil tank allowed the dyed tracer to be visually tracked using digital photography during the experiments. This facilitated the determination of the general boundaries of the plume as it spreads and helped informing sampling strategies. A screened layer of pea gravel, 10-cm thick, was placed at the top and bottoms of both ends of the soil tank to control the head gradients (Figure 2b); in the first two experiments, a series of constant-head reservoirs was connected to them to adjust the head level. These boundary conditions (BCs) will be referred to henceforth as "experimental BCs." In the third experiment, a long well was installed in the gravel section located at the top of Zone 3 from which water was extracted at a fixed rate by a peristaltic pump (Cole-Parmer Masterflex L/S: 7526-60). It should be noted that while steady-state flow was the objective, some minor transient flow was still observed.

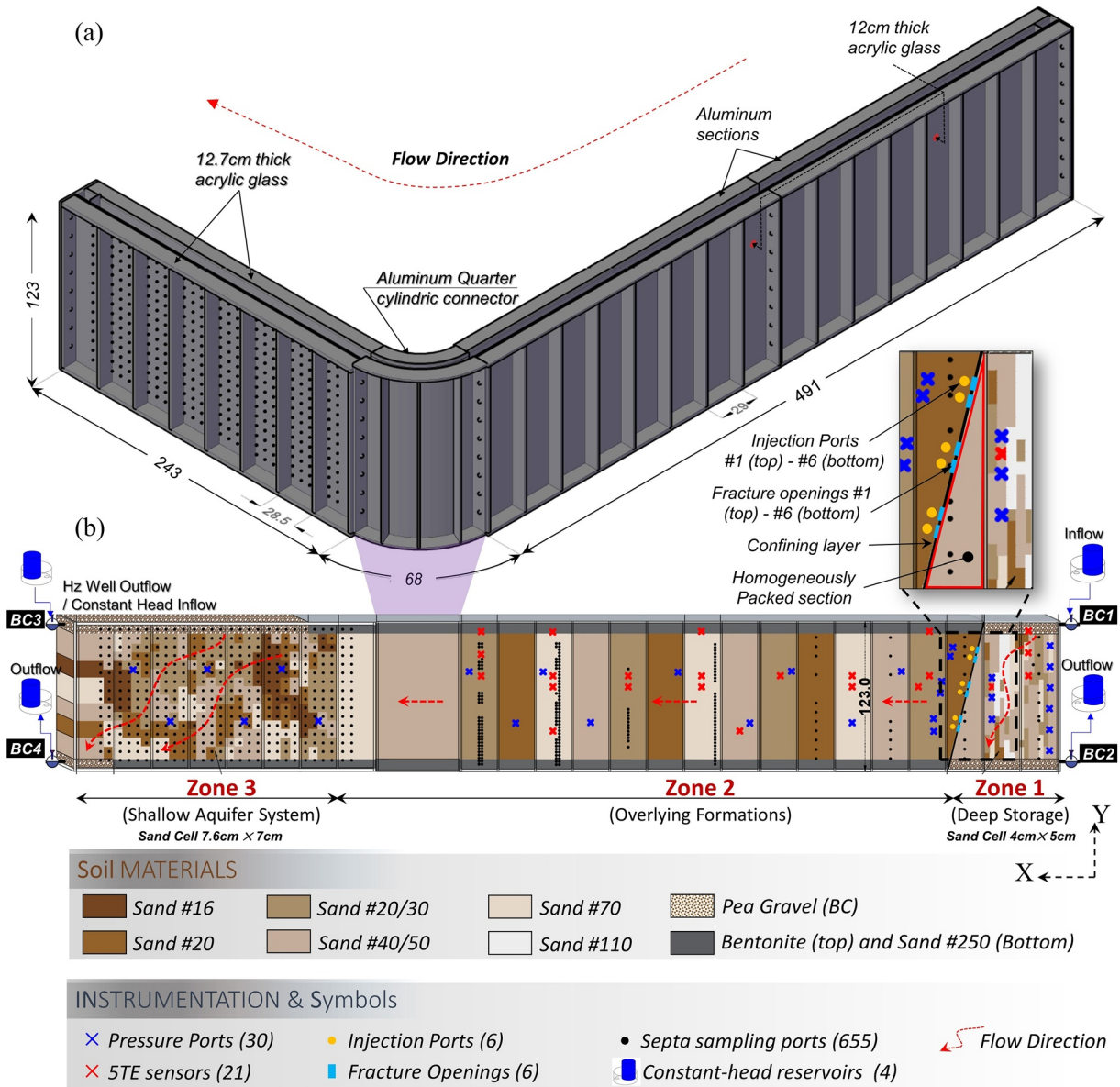

Figure 2. Depiction of (a) the soil tank, (b) instrumentation layout and packing configurations. All dimensions are in centimeters. The numbering scheme for the injection ports, instrumentation, and sampling ports increases sequentially from top to bottom and right to left. Flow occurs from right to left.

One wall of the acrylic section of the tank containing Zone 3 had a 16 × 30 rectangular grid of 7.0 cm wide squares. A self-sealing septa port was installed at each intersecting point of the grid for high-resolution (480 individual points) aqueous sampling with syringes (Figure 2b). An additional 175 septa ports were installed at a much coarser resolution in Zones 1 and 2. A total of 30 piezometers were installed across the tank (Figure 2b) with the highest spatial distribution near the brine injection point so as to detect pressure changes due to tracer injection. A total of 21 electrical conductivity sensors (5TE-Decagon Devices) were installed in Zones 1 and 2 to automatically track plume propagation. A 2.2 cm thick acrylic sheet with a width equal to that of the internal width of the soil tank was installed at an angle of 76° to represent an impermeable caprock. Prior to its installation, six 4 cm holes were drilled in the sheet (Figure 2b) to simulate fractures within the damaged zone of a caprock. The inclined confining sheet was modeled after the upward dipping caprock (Freeman Shale) of the potential CO_2 storage (Vedder formation) in Southern San Joaquin Basin, California (Cihan et al., 2015). This inclination induced nonuniform fluid fluxes at the inflow and outflow boundaries of Zone 1, which in-turn created a complex flow filed at this zone and at the source vicinity. Six

Table 1
Physical Properties of Sands Used in Soil Tank

Sand no.	#110[a]	#70[b]	#40/50[c]	#20/30[b]	#20[b]	#16[b]
Porosity [m^3/m^3]	0.340	0.413	0.334	0.406	0.410	0.397
d_{50} [mm]	0.103	0.2	0.35	0.54	0.70	0.88
Dry bulk density [g/cm^3]	1.75	1.56	1.55	1.57	1.56	1.60
Saturated K[d] [m/day]	5.52	12.10	44.93	101.95	181.44	476.93
ln(K) [–]	1.70	2.5	3.80	4.6	5.20	6.2

Note. Data extracted from Agartan (2015), Barth, Hill, Illangasekare, and Rajaram (2001), Peng and Brusseau (2005), and Sakaki and Illangasekare (2007).
[a]US Silica Co. [b]Unimin, Corp. (Granusil sand). [c]Unimin, Corp. (Accusand sand). [d]K values are based on column-scale laboratory testing.

external injection lines were similarly installed at a distance of 5 cm from the holes to inject the bromide tracer at distinct rates and locations during the experiments.

2.3. Soil Packing Configuration

The soil tank was packed with six well-characterized manufactured silica sands (see Table 1 for properties) to create the layered system shown in Figure 2b. The packing configurations applied in Zones 1 and 3 were designed to resemble natural sedimentary strata. The approach used to develop the discrete heterogeneity fields was designed to ensure that predefined geostatistical structures are honored (Barth, Hill, Illangasekare, & Rajaram 2001; Trevisan et al., 2017). The sequential indicator simulator in SGeMS (Deutsch, 1998; Remy et al., 2009) was used to generate two sets of 200 unconditional realizations with correlated lognormal hydraulic conductivity (lnK) fields for Zones 1 and 3. The final packing configuration was selected for each zone based on a two-stage selection criterion. First, realizations exhibiting normal distributions of lnK and smooth semi-variograms were drawn from the full set. These realizations were then represented in a FEFLOW transport and flow model, described in Section 3, to identify which configuration provides the most nonuniform streamlines in Zone 1 and widest distributed plume in Zone 3. The selected discrete configurations for packing were found to reasonably approximate the target continuous distributions of lnK designed for Zones 1 and 3 (Figure S1).

The heterogeneity (defined in terms of permeability) of Zone 1 had a lnK normal distribution with a mean (μ_{lnK}) of 3.8, variance (σ^2_{lnK}) of 1.1, and correlation scale (λ_{Hz}/λ_V) of 3.16. While, Zone 3 had a μ_{lnK}, σ^2_{lnK}, and λ_{Hz}/λ_V values of 4.6, 2.0, and 1.6, respectively. These geostatistical parameters were comparable to field data at well-characterized sites (Garabedian et al., 1991; Hess et al., 1992; Rehfeldt et al., 1992). It should be noted that a part of Zone 1 located immediately next to the inclined caprock (encircled by red line in the inset part of Figure 2b) was homogeneously packed out of necessity given the limited access to this confined area in the tank.

In Zone 2, a nonstationary structure was assumed due to the extreme depth being emulated (>1.0 km) and the expected uncorrelated discrete geological layering associated with natural, sequential deposition and weathering in this section. Therefore, this Zone was packed variably with sand ranging from #20 to #70 (Figure 2b). This packing configuration was inspired by the nearly perfect layered stratigraphy of the Utsira Formation, a target CGS reservoir located at the Sleipner field in the North Sea (Hermanrud et al., 2009; Torp & Gale, 2004; Zweigel et al., 2004). Tank packing procedures can be found in Text S1 in the Supporting Information S1.

2.4. Tracer Properties and Sampling Strategy

Sodium bromide (NaBr), a conservative tracer under laboratory conditions (i.e., pH, temperature, and pressure), was selected as a surrogate for the leaking brine. The total volume of tracer solution, specific to each experiment, was prepared before the experiments and stored in a plastic drum, equipped with in-house developed stirring and cooling systems, to maintain a consistent tracer concentration. NaBr tracer solution was prepared for Experiments 1, 2, and 3 by mixing 5.6, 7.24, and 11.22 g of granular NaBr salt

Table 2
Summary of Experimental BCs and Collected Data Statistics

Exp. no.	Inj. port[a]	Boundary conditions[b]	NaBr conc. (mg/l) (Count)	Injection rate (ml/min) (Count)	Collected data density		
					Aqueous samples	Head records	Inflow and outflow[c]
Exp-1	3	BC1 = 165.44 cm, BC2 = 164.47 cm, BC3 = 161.15 cm, BC4 = 150.50 cm	42.4 ± 2.4 (17)	7.45 ± 0.04 (17)	423	570	24
Exp-2	1	BC1 = 165.44 cm, BC2 = 164.47 cm, BC3 = 161.15 cm, BC4 = 150.50 cm	54.5 ± 2.6 (18)	7.9 ± 0.06 (19)	582	480	35
Exp-3	6	BC1 = 165.10 cm, BC2=No-Flow, BC3 = 8.3 ml/min, BC4 = 157.9 cm	85 ± 4.7 (22)	7.9 ± 0.1 (24)	1,767	540	58

Note. Inj., injection.
[a]Injection ports #3, #1, and #6 are located in the middle, top, and bottom of tank height, respectively. [b]BC numbers are identified in Figure 1. [c]The number of measurements of the system inflows and outflows at Zones 1 and 3 are usually equal.

(102.9 NaBr/mol–Mallinckrodt 0535) with 102 l of bromide-free tap water (water quality was evaluated internally), respectively. The NaBr tracer was doped with a 0.03% concentration (by volume) of a blue dye (Envision DYEBLU-GL) in the first experiment and florescence dye (ACROS-Organics 17,324-5000) in the second and third experiments to visually track the plume migration from the transparent side of the tank and develop sampling strategies as will be discussed later. The decision of using florescence dye in the later experiments was due to the observed high retardation of the blue dye compared to NaBr tracer which affected the sampling strategy in Experiment 1. The electrical conductivity of the prepared solution in the drum was monitored with a conductivity meter (OAKTON-CON 100 series) to identify when the concentration of the solution is uniform and ready for injection. The concentration of NaBr solution was designed based on non-dimensional density instability relationships (Barth, Illangasekare, Hill, & Rajaram, 2001; Oostrom et al., 1992). The results of this non-dimensional analysis were further tested and validated in density-dependent FEFLOW simulations to determine what concentration triggers the onset of this instability. This analysis showed that using NaBr solution concentration in a range of 0–100 mg/l will create negligible instability-sinking conditions for the plume moving in the horizontal direction of the tank. Therefore, NaBr tracer used in the three experiments had a concentration within that range as shown in Table 2.

Aqueous sampling was determined in real-time during the experiments by visually monitoring the plume location; sampling was performed within the plume to a 20 cm extent from its boundary. A sampling volume of 0.5 ml was extracted from each targeted septa port with a syringe. The small extraction volume ensured that the flow field was not disturbed by the extraction process. Given the total volume of tracer used during each experiment, the mass removed from the system during sampling can be considered negligible, roughly 0.5% of the total amount of injected tracer. The collected samples were stored in 0.9 ml vials, sealed with parafilms, and placed in a refrigerator for preservation. These samples were later chemically analyzed using an ion chromatography (IC) system (Dionex Aquion combined with autosampler Dionex As-Dv). To ensure the fidelity of the measurements, the guidelines of Hautman and Munch (1997), Christison et al. (2016), and U.S. EPA (2016) were rigorously followed. Nine calibration solutions (0.1, 0.5, 1, 5, 10, 25, 50, 75, and 100 mg/l of Br) were prepared by diluting stock standard solutions with 1,000 and 50 mg/l of Br (Inorganic Ventures IV-STOCK-59/64) to develop the calibration curves of the IC prior to every run of the machine.

2.5. Experiment Procedures

A series of three experiments were conducted as part of this study. In each experiment, the boundary conditions shown in Table 2 were applied to develop the ambient flow field in which different unique scenarios of plume migration were created by varying the injection rates and locations. The maximum hydraulic gradients induced by the assigned boundary conditions were 0.018, 0.018, and 0.009 for Experiment 1, 2, and 3, respectively. A summary of the injection ports, average concentrations of injected NaBr tracer, average injection rates, and density of collected data can be found in Table 2. Upon adjustment of the constant head devices and the establishment of steady flow, the tracer solution was injected at the downstream exit of the openings in the caprock using a peristaltic pump (Cole-Parmer Masterflex L/S Peristaltic Pump 7526-60) at a rate that varied between 7.5 and 8.0 ml/min. Hydraulic heads, system inflow, outflow, tracer injection

rate, and injection concentration were measured at least twice a day to monitor temporal variations. A large number of tracer samples were collected during the three experiments as shown in Table 2. These data were used to generate high-resolution spatiotemporal concentration breakthrough curves (BTCs) that were in turn used for model calibration and validation. The temporal durations of Experiments 1, 2, and 3 were 204, 194, and 190 h, respectively. It is noteworthy that data generated from the three experiments were used also in a different study focusing on validating a new transport inverse method developed by Jiao et al. (2019).

3. Numerical Modeling

A large number of transport codes use the conventional coupling of Darcy's (1856) law with the advection-dispersion equation (ADE), based on the Fickian transport assumption (Bird et al., 1960; Taylor, 1953), to simulate solute transport. The ADE has been shown to be inadequate in some cases however, as it can fail to capture the transport processes due to scale-dependent dispersion coefficients, heavy tailing of the BTCs and directional/time-variant porosity (Willmann et al., 2008); this has led to the development of modifications to the ADE to describe non-Fickian plume behavior (Benson et al., 2000a, 2000b; Schumer et al., 2001, 2009; Zhang et al., 2007, 2008, 2009) which in natural systems, can be caused by the presence of complex geological settings and soil heterogeneity. In deep subsurface regimes (e.g., brine leakage problem), modeling groundwater flow and transport is even more sophisticated due to the existence of many interplaying physical processes at multiple layers that creates multidimensional flow fields; these processes include fracture flow, density effects, varying material properties, and zones with unsaturated flow (Ramadas et al., 2015). Comprehensive prior information and field data are therefore required to validate models used for addressing problems located in deep systems.

In the context of the present study, Saiers and Barth (2012) and Cohen et al. (2013) questioned the applicability of a MODFLOW-based model (Zheng & Wang, 1999) used by Myers (2012) to evaluate the potential risk of formation brine leakage based on oversimplifying the system flow field and specifying unrealistic model boundary conditions–all of which could not be adequately validated with field data. Yamamoto et al. (2009) further noted that models simulating pressure field perturbations caused by CO_2 injection (i.e., leakage onset) should include an accurate description of the shallow and deep subsurface system characteristics. The use of ADE-based codes that can account for density-dependent flow (e.g., MODFLOW/MT3DMS or FEFLOW) to simulate leaking brine migration across a multilayered system is predicated on their ability to capture complex multidimensional flow fields. Model validation requires extensive long-term field data collected at high spatiotemporal resolutions for sites whose geology has been well characterized (Jiang, 2011; Ramadas et al., 2015; Tsang et al., 2008). Given that deep subsurface datasets of this nature may not be available, the laboratory data generated in the well-controlled intermediate-scale experiments in this study were used to calibrate and validate a FEFLOW transport model developed to simulate leaking brine.

3.1. Model Setup, Calibration, and Validation

FEFLOW (V 7.1) was selected as the single-phase flow and transport code to develop a model for simulating brine leakage experiments as recommended by Cihan et al. (2013). FEFLOW is a finite element method (FEM) code that discretizes the solution domain and solves the coupled groundwater flow and transport equations in a continuous FEM scheme. To ensure local mass conservation in FEFLOW, the continuous FEM is enhanced by local smoothing techniques and consistent velocity approximator (Diersch, 2014).

A 2D flow and transport model was developed in FEFLOW for the packing configuration presented in Figure 2b to simulate tracer transport in the steady-state flow field of the test tank; steady-state flow conditions were assumed so as to reduce the computational burden of the optimization process. To validate the 2D assumption for the problem, a local 3D model was developed for the vicinity of the injection ports and across the openings' system, the most critical part for the plume evolution, and the resulted water and mass fluxes were compared to the 2D model. A difference less than 1% between the results of the two models was obtained. Isothermal conditions were also assumed in the model due to the limited temperature fluctuation observed in the experiments (±2°C). Reducing model dimensions from 3D to 2D and the assumed isothermal conditions helped in limiting the computational cost of the model calibration process.

The assigned boundary and initial conditions were varied between simulations following those applied during each experiment (Figure S2). The Péclet number was larger than 10^2 in Zones 2 and 3 (transport domain), indicating that the plume transport was advection dominated. Based on high-resolution digitized photographs of the packed sands, K heterogeneity was explicitly represented in the flow model, where model domain was discretized by 167,207 triangular elements with average nominal sizes of 0.6 ± 0.16 cm^2. Local mesh refinement was implemented at the tracer source area to enhance model convergence, which resulted in an element size as small as 7×10^{-4} cm^2.

Within the computed steady-state velocity field, tracer transport was modeled by solving the ADE with a constant averaged NaBr mass flux assigned at the prescribed source location. Neglecting the observed slight fluctuation in the measured tracer injection rate led to obtain a better fit to observation data; Thornton et al. (2013) recommended a similar simplification for simulating contaminant source discharge with short-term fluctuation conditions. Loss of solute due to tracer sampling was considered negligible and not accounted for the modeling efforts. The predictor-corrector time integrator introduced by Gresho et al. (1979) and improved by Bixler (1989) was used to discretize the time and progressively optimize the length of time steps—this scheme reduced the transport model computational burden with minor effect of numerical dispersion. The model was queried at the same times that the experimental samples were taken so as to produce comparable concentration fields.

The column-scale K values presented in Table 1 were initially assigned as the soil properties in the model. Longitudinal dispersion coefficients (α_L) of 0.12 and 0.05 cm were respectively specified for Zones 2 and 3 based on the empirical formulations of Neuman (1990). Transverse dispersion coefficients (α_T) were assumed to be 10% of the longitudinal dispersion coefficients (Gelhar et al., 1992). Meanwhile, Zone 1 was assigned α_L and α_T values of 0.1 and 0.07 cm, respectively. Despite the good fit to hydraulic head data (error ~1 mm), significant discrepancies in the shape and position of the simulated plume were observed. Possible explanations include: (a) upscaling errors associated with the use of column-scale K values (Barth, Hill, Illangasekare, & Rajaram, 2001; Rovey, 1998), (b) the six caprock fractures may have had nonidentical K values as their screens rusted nonuniformly over time, and (c) the permeability of the four pea gravel sections, used to control the boundary conditions, may not be identical. These initial simulation results therefore prompted the detailed model calibration described below.

The nonlinear regression algorithm of PEST (Doherty, 1994, 2015; Doherty et al., 2010) was used to optimize model parameters. FePEST, a graphical user interface that links the open-source parameter estimation package of PEST and BeoPEST (Hunt et al., 2010) to FEFLOW, was specifically used in this effort. With the advances of BeoPEST, an in-house parallel computing system (8PCs with quad-core CPUs at 3.4 GHz each) was used to reduce the computational burden of inversion. Data from Experiments 2 and 3 were used for calibration and Experiment 1 for final validation. A linear sensitivity analysis revealed that K, dispersion coefficients, and porosity (ϕ) were the most influential parameters in the model - in agreement with previous studies (Sarris et al., 2018; Yoon & McKenna, 2012). Thus, PEST was set to run forward models of Experiments 2 and 3 simultaneously and iteratively to reduce the overall objective function by finding the optimum identical values of these parameters that enhances the model fit to both datasets. In the inversion problem, zonal parameterization was used to explicitly represent the spatial distribution of target parameters (K, $\alpha_{L,T}$, and ϕ) according to the experimental packing. Details about zones and bounds that were considered for each parameter is presented in Table S1.

The calibrated model's performance was appraised using different metrics. Scatter plots were used to compare simulated concentrations with observed values. Percent absolute error (PAE) quantified the deviation of simulated system state variables (i.e., hydraulic head and inflows/outflows) from the experiments. Normalized root mean square error (NRMS) similarly was calculated to evaluate the error of simulated concentration data. PAE and NRMS are defined respectively as follows:

$$PAE = \left| \frac{V_m - V_s}{V_m} \right| \times 100 \quad (1)$$

$$NRMS = \frac{\sqrt{\sum \left(C_m - C_s \right)^2 / n}}{C_0} \quad (2)$$

where V_m is a measured state variable of flow (i.e., transient hydraulic head and outflows), V_s is the simulated state variable of flow (i.e., steady state heads and inflows/outflows), C_m is measured concentration, C_s is simulated concentration, C_0 is tracer concentration at the source, and n is sample size. Note that the error was defined as the difference between observed and simulated values at the same location and time in both the experiments and the simulations.

Temporal and spatial moment analyses (Farrell et al., 1994; Fetter et al., 2017; Freyberg, 1986) were also conducted so as to test the model's ability to capture the most critical characteristics of the plume to this study (e.g., plume mean arrival time and center of mass and spread). For this analysis, the first temporal and spatial moments normalized by the zeroth moments were used to determine the mean arrival times and the mass center of the simulated and observed plumes. The normalized second spatial moments were used to determine the longitudinal and transverse plume spreads from their centers of mass. Moment calculations were performed for the entire plume across Zones 2 and 3.

4. Results and Discussion

4.1. Experimental Results and Model Performance

Although the model used in this study assumes steady-state flow conditions, it was compared to the experimental transient data collected on the system state variables including: the twice-daily measured hydraulic heads, inflows, and outflows. Figure 3a presents the maximum, minimum, and median of PAEs associated with each system state variable as measured over the duration of the experiments. Simulated hydraulic heads showed a very good fit compared to observed data with a maximum PAE ≤0.7%. Median PAEs in the predicted inflow and outflow of Zones 1 and 3 in Experiments 2 and 3 were ≤15%, except for Zone 1 outflow in Experiment 2. The outflow from Zone 1 in Experiment 2 was affected by the accumulation of rust on the screens of the pea gravel section at BC2 (Figure 2b). Therefore, this outlet was subsequently disabled in Experiment 3. During Experiment 1, the effluent rate from Zone 3 was observed to decrease gradually over time as a result of a clogging in the outlet connected to BC3 (Figure 2b). Analysis of the simulation results showed that a transient flow-type boundary condition should be assigned to Zone 3 outlet in the forward model (Figure S2b) to improve the hydraulic head predictions. It should be noted that the effluent rates from Zone 1 were not measured during Experiment 1.

Goodness-of-fit between simulated and observed plume concentrations are represented in Figures 3b–3d. The plume concentrations were well predicted as can be seen in the NRMS values of 0.098 in Exp.1, 0.105 in Exp.2, and 0.083 in Exp.3. Despite having large datasets and a well characterized system to work with, reproducing observed transport data remains difficult. Barth, Hill, Illangasekare, and Rajaram (2001) and Yoon and McKenna (2012) described such model-to-measurement discrepancies as inevitable because of the uncaptured sub-grid scale processes introduced by micro-heterogeneity in the tank packing. From our observations, other reasons can be included; variations in the upstream and downstream effluent rates, variability in the tracer injection rate, possible non-steady flow in the immediate vicinity of the caprock fractures which enhances transverse dispersion, standard error margin of the IC analysis (1%–2%), the non-point-like measurements of plume concentrations (average concentration over the 0.5 ml extracted volume), and potential error in the defined observation locations in the model (1–2 mm).

The slight variability in plume position over time due to the nonsteady flow at the leakage source (Table 2), distorted the BTCs of the septa ports located at the plume fringe and front. Although, extremely distorted data points were excluded from the calibration dataset to avoid failure in the optimization process, remained data used for calibration included some slightly distorted BTCs. This distortion was most pronounced in the data of Experiment 2 because of the partial clogging associated with BC2 (Figure 2b), which induced nonsteady conditions at the source and caused large NRMS. Examples of slightly to highly distorted concentration data from Experiment 2 are presented in Figure S3.

The spatial moment analysis of simulated and observed plumes revealed an average PAE of 0.43% in the location of the plumes' centers and 10% in their widths. The temporal moment analysis showed that the model was able to reproduce the mean arrival times of the three plumes at the sampling locations of Experiments 1, 2, and 3 with an average PAE of 0.4%, 2.7%, and 1.8%, respectively. Figure 4 presents a visual comparison between observed and simulated plume arrival times as contour lines, which overlay spatial maps

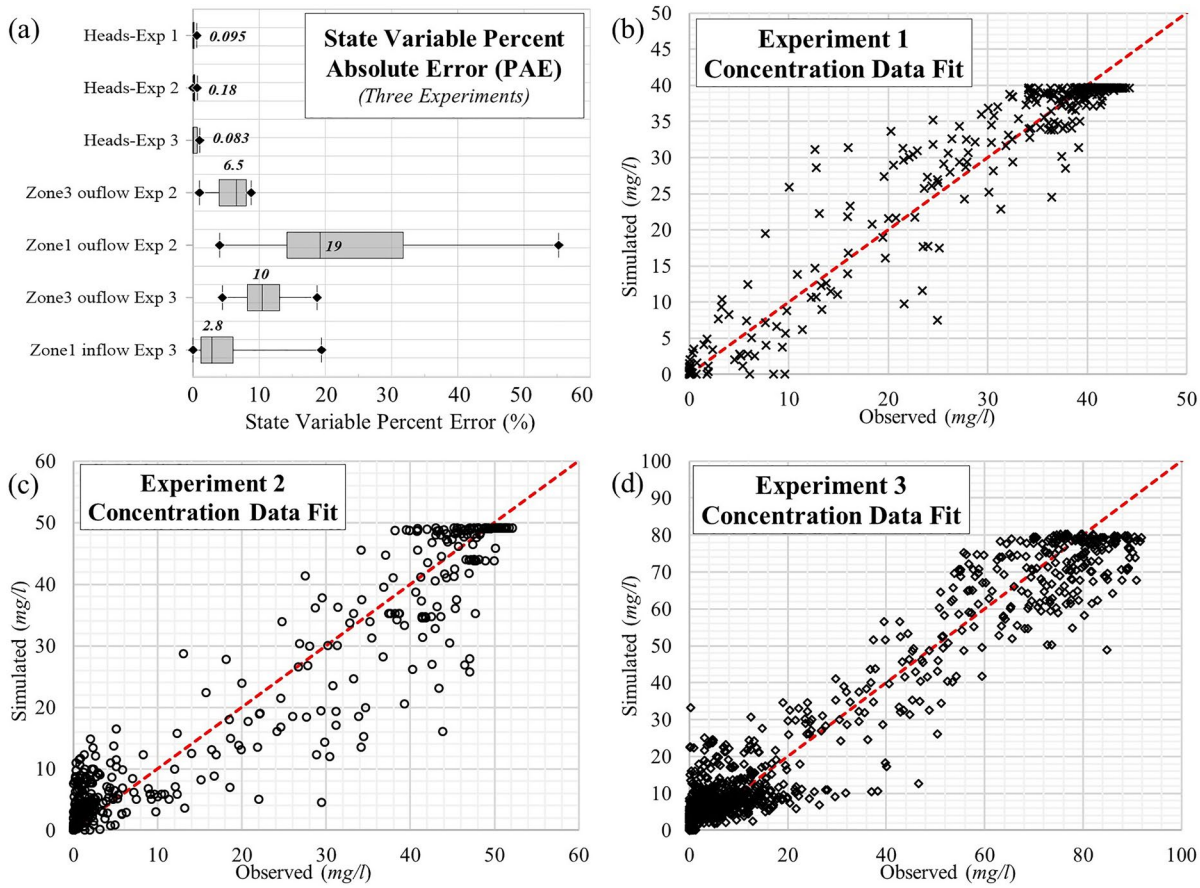

	NRMS	Error Mean (μ)	Error STD. (σ)	# Data points
Experiment 1	0.098	0.096 mg/l	4.19 mg/l	321
Experiment 2	0.105	-0.065 mg/l	5.76 mg/l	456
Experiment 3	0.083	-1.2 mg/l	6.90 mg/l	1575

Figure 3. (a) Calculated percent absolute error (PAE) for each calibrated flow variable with the median (50th percentile) value shown and (b–d) observed versus calibrated concentration data for each experiment. Table includes Normalized Root Mean Square (NRMS), sample size, mean, and standard deviation (SD) of the residuals.

of the final calibrated parameters. As shown in Figure 4, a high porosity value (0.6) was assigned to the #70 fine sand in Zone 2 to match the experimental arrival times. This was caused by packing errors in Zone 2; when dividers were raised to pack the next level in the tank, small portions of sand were blended with the neighboring cells (e.g., sand #20 and sand #70 cell mixed at their interfaces). This created thin (~4 mm thick) layers with different permeability which as a result, introduced unaccounted local micro-heterogeneity. Plumes encountered this micro-heterogeneity branched out (Figure 3), varying the arrival times of the plumes at ports located in the same sand type significantly. This in turn misinformed PEST, causing the algorithm to unrealistically adjust the porosity to fit the data. However, it is worth mentioning that this porosity field led to a reasonable prediction of the mean arrival times of the validation Experiment #1.

Ensuring that the model was able to capture the flow field of Zone 1 is an important consideration as the primary focus of this study is the exploration of how inaccurate information about the storage formation impacts simulation results. This was addressed by comparing the simulated and observed flow fields in Zone 1 and at the source vicinity. In this test, a bromide-free dye tracer was injected at a few locations in Zone 1 and around the fractures so that the experimental flow field could be delineated. The resulting tracer trajectories were compared to the streamlines of the model in the same zones. The good fit between observed and simulated flow fields in Zone 1 and source vicinity (Figure S4) revealed the ability of the calibrated model to reproduce the physical processes controlling NaBr migration in the tank while fitting

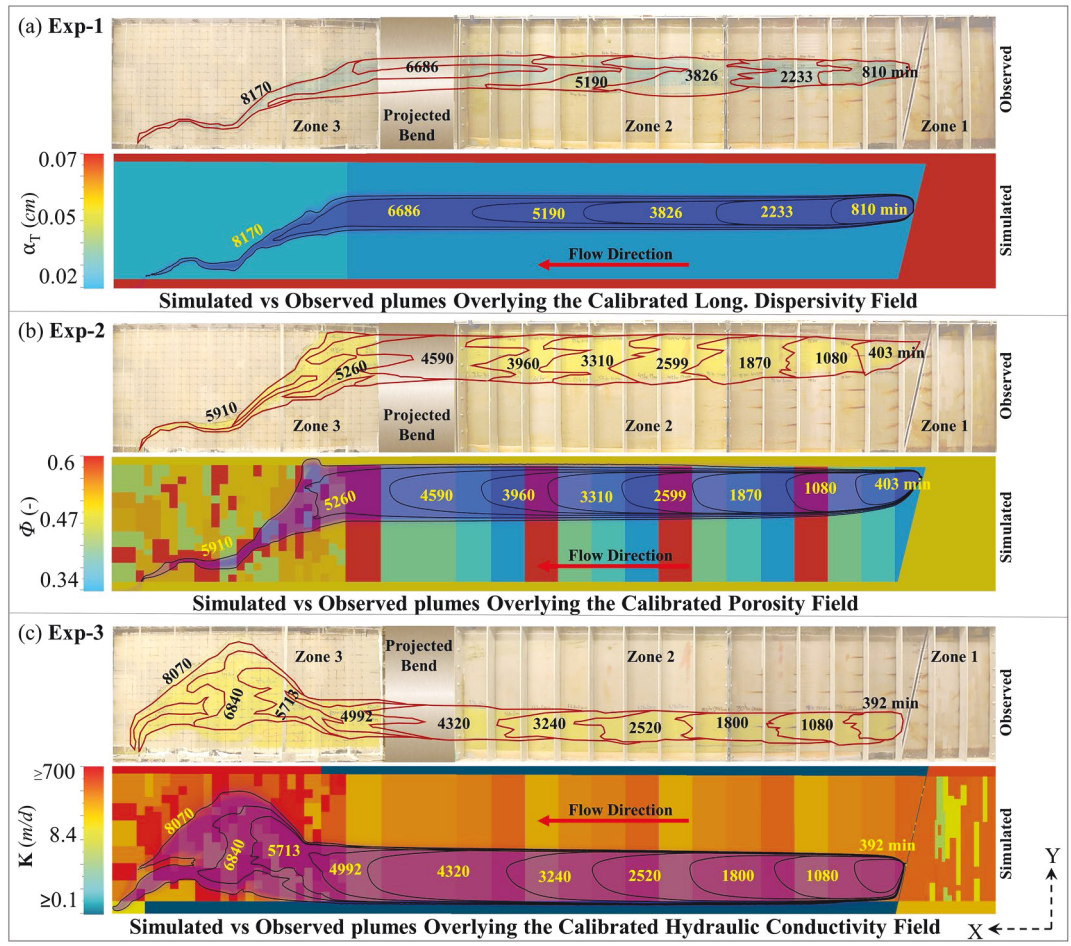

Figure 4. Visual comparison between observed and simulated plume distributions which overlay spatial maps of the final calibrated parameters [hydraulic conductivity (K), porosity (ϕ), and transverse dispersion coefficients (α_T)] in (a) Experiment 1, (b) Experiment 2, and (c) Experiment 3.

observed data. Based on above discussion, the validated flow and transport model was verified as an analog for the physical experiment and could therefore be used to explore the impacts of different scenarios of uncertainty in source conditions.

4.2. Numerical Experiments

In order to explore the impact of source condition uncertainties, the validated model was used to create a hypothetical reference scenario (Figure 5a) based on the physical dimensions of the soil tank and calibrated parameters (Figure 4). In this scenario, we rotated the model domain back by 90° to simulate the brine migration under the density contrast effects expected in the field, which was manipulated in the tank to enable laboratory experimentation. The authors recognize that the brine leakage plume predicted under the chosen modeling scale is likely to be specific to the simplified experimental settings of this study. Much like other CGS intermediate-scale studies (e.g., Plampin et al., 2017; Trevisan et al., 2017), we believe that important insights for modeling the full-scale problem can still be drawn. Moreover, upscaling the model parameters that were calibrated using experimental data to field dimensions was considered invalid to avoid introducing scaling errors. Nevertheless, this analysis can still shed the light on the important source conditions that need to be well-characterized to reasonably predict the brine leakage migration pathways and areas likely to be impacted in the shallow aquifer.

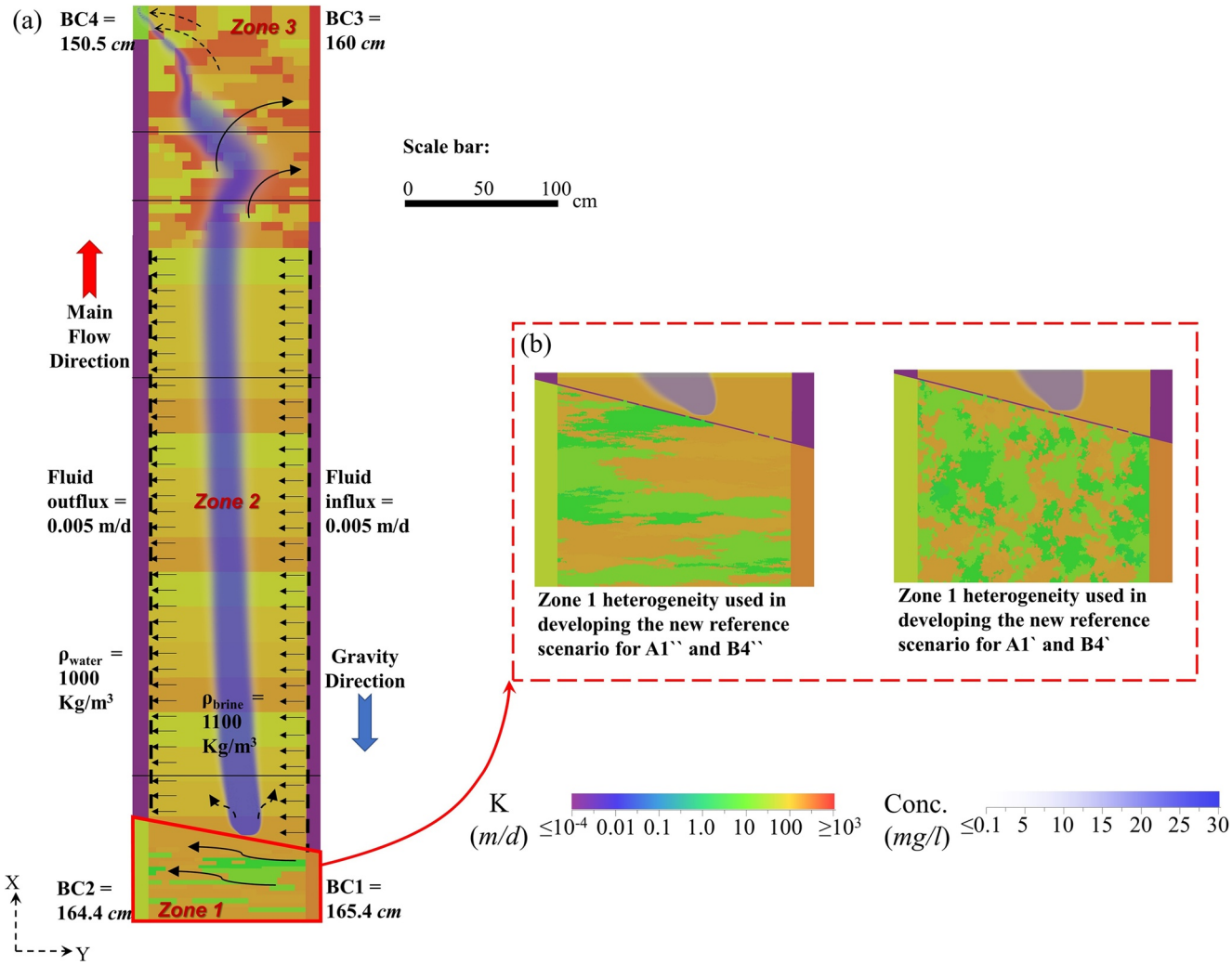

Figure 5. (a) The simulated steady state plume in the reference scenario ("reference plume") showing the assigned BCs. (b) Zone 1 heterogeneity used to develop the new reference scenarios. *Note*. The direction of flow is from bottom to top and all outer boundaries were assigned no-flow BCs unless otherwise stated.

In the analysis presented below, the effects of altering source conditions on the relative change of the brine plume distribution is quantified by comparing the simulation results against those of the developed reference scenario. This scenario applied the same boundary conditions as Experiment 1, except the hydraulic head at BC3 that was lowered to 160 cm so as to ensure that the plume does not approach the boundaries of Zone 2 after including a lateral flow of 0.005 m/day at Zone 2 (Figure 5a). It should be noted that the lateral flow in Zone 2 was applied only in the numerical experiments. The densities of the native brine and overlying groundwater were assumed to be 1,100 and 1,000 kg/m^3, respectively (Birkholzer et al., 2011; Sun, Zeidouni, et al., 2013; Zhou et al., 2010). Steady-state flow and transport simulations were considered satisfactory for this analysis as risk assessment is typically informed by the eventual distribution of the brine plume.

The overall uncertainty analysis was composed of 46 different scenarios, categorized under 5 possible cases of uncertainty, in which various hydraulic and geometrical parameters were adjusted. Descriptions of different types of tested scenarios are provided in Table 3. The scenarios were divided into two primary groups (denoted A and B) according to the location where the system parameters were adjusted; parameters included the hydro-structural settings of the storage zone (group A) and caprock fractures (group B). The impact of the changes associated with each scenario was quantified in terms of the relative error, which accounts

Table 3
Summary of the 46 Tested Uncertainty Scenarios

Uncertainty location	Scenario ID	Scenarios description	
Storage formation (Group A)		Case 1: Assuming homogeneous storage formation (5 scenarios)	
	A1–A3	Independently, assigning well-estimated, halved, and doubled equivalent ln$K$ in Zone 1	
	A1′ and A1″	Assuming homogenous ln$K$ to represent two more heterogeneous permeability fields of Zone 1	
		Case 2: Storage formation geostatistical parameter uncertainties (24 scenarios)	
		Assumed uncertainty in three tested realizations	Geostatistics
	A4–A6	Identical geostatistical parameters to original reference scenario	($\lambda_V/\lambda_{Hz} = 35/11$, $\sigma^2_{lnK} = 1.0$, $\mu_{lnK} = 3.8$)
	A7–A9	Uncertainty introduced through decreasing the mean ln$K$ (μ_{lnK})	($\lambda_V/\lambda_{Hz} = 35/11$, $\sigma^2_{lnK} = 1.0$, $\mu_{lnK} = 2.5$)
	A10–A12	--- " --- through increasing the variance of ln$K$ distribution (σ^2_{lnK})	($\lambda_V/\lambda_{Hz} = 35/11$, $\sigma^2_{lnK} = 3.5$, $\mu_{lnK} = 3.8$)
	A13–A15	--- " --- through decreasing the μ_{lnK} and increasing the σ^2_{lnK}	($\lambda_V/\lambda_{Hz} = 35/11$, $\sigma^2_{lnK} = 3.5$, $\mu_{lnK} = 2.5$)
	A16–A18	--- " --- through decreasing the transverse correlation length (λ_V)	($\lambda_V/\lambda_{Hz} = 11/11$, $\sigma^2_{lnK} = 1.0$, $\mu_{lnK} = 3.8$)
	A19–A21	--- " --- through decreasing both λ_V and μ_{lnK}	($\lambda_V/\lambda_{Hz} = 11/11$, $\sigma^2_{lnK} = 1.0$, $\mu_{lnK} = 2.5$)
	A22–A24	--- " --- through increasing λ_V	($\lambda_V/\lambda_{Hz} = 80/11$, $\sigma^2_{lnK} = 1.0$, $\mu_{lnK} = 3.8$)
	A25–A27	--- " --- through decreasing both λ_V and μ_{lnK}	($\lambda_V/\lambda_{Hz} = 80/11$, $\sigma^2_{lnK} = 1.0$, $\mu_{lnK} = 2.5$)
		Case 3: Uncertainty in storage formation boundary conditions (3 scenarios)	
	A28–A30	Independently, increasing BC1 by 2%, lowering BC2 by 2%, and lastly considering both errors (varying BC1 by +2% and BC2 by −2%)	
Caprock Fractures (Group B)		Case 4: Uncertainty in fracture hydraulic conductivities (K_{fracs}) (8 scenarios)	
	B1–B3	Independently, doubling K_{fracs}, halving $K_{fracs,}$ and reversing the order of K_{fracs}	
	B4–B6	Independently, representing all fractures by an equivalent single pathway ($K_{eq.fracs}$), halving $K_{eq.fracs}$ and doubling $K_{eq.fracs.}$	
	B4′ and B4″	Assuming an equivalent single leakage pathway when two more heterogeneous permeability fields were considered in Zone 1.	
		Case 5: Poor characterization of fracture structural settings (6 scenarios)	
	B7–B9	Independently, moving all fractures 5 cm upward, 5 cm downward, and moving the two middle ones 5 cm apart	
	B10–B12	Independently, doubling, halving all fracture sizes, and doubling the size of the middle ones only	

Note. Adjusted variables are Zone 1 ln$K$, σ^2_{lnK}, μ_{lnK}, λ_V, BCs, K_{fracs}, and $K_{eq.fracs}$. Scenarios A1′, A1″, B4′, and B4″ (gray-shaded) relied on different reference scenarios as shown in Figure 5.

[a]Details in each line in the table, respectively, describe the induced uncertainty in each scenario stated in the second column of the table.

for errors in the predicted spread and pathway of the brine plume. We used a Cartesian (X, Y) coordinate system in which X corresponds to the streamwise longitudinal direction and Y corresponds to the transverse (relative to primary flow) direction (Figures 4 and 5). The plume mass center (Xc and Yc) and spread (XXc and YYc) in the uncertainty scenarios, calculated using spatial moment analysis, were compared to the reference plume using Equation 3:

$$Relative\ Error\ for\ Z\left(RE_Z\right) = \left|\frac{Z_{Reference\ plume} - Z_{Uncerinity\ scenario}}{Z_{Reference\ plume}}\right| \times 100 \quad (3)$$

where (Z) is an arbitrary variable that can represent any of the normalized spatial moments, Xc, Yc, XXc, and YYc. To recognize changes in the geostatistical parameters in scenarios A7–A27 in Table 3, we recall that the original geostatistical parameters of the implemented heterogeneity in Zone 1 in the soil tank and reference scenario were $\lambda_V/\lambda_{Hz} = 35/11$, $\sigma^2_{lnK} = 1.0$, and $\mu_{lnK} = 3.8$. Owing to the packing limitations described in Section 2.3, the implemented heterogeneity in Zone 1 included a homogenous part upstream of the fractures (highlighted red in Figure 2). This part can create a uniform flow prior to the fractures and impact our evaluation of the errors associated with assuming a homogeneous storage formation or a single leakage pathway (Scenarios A1 and B4). To ensure efficient evaluation of these errors, two new reference scenarios underlying more heterogeneous ln$K$ field and occupying the full area of Zone 1 were developed

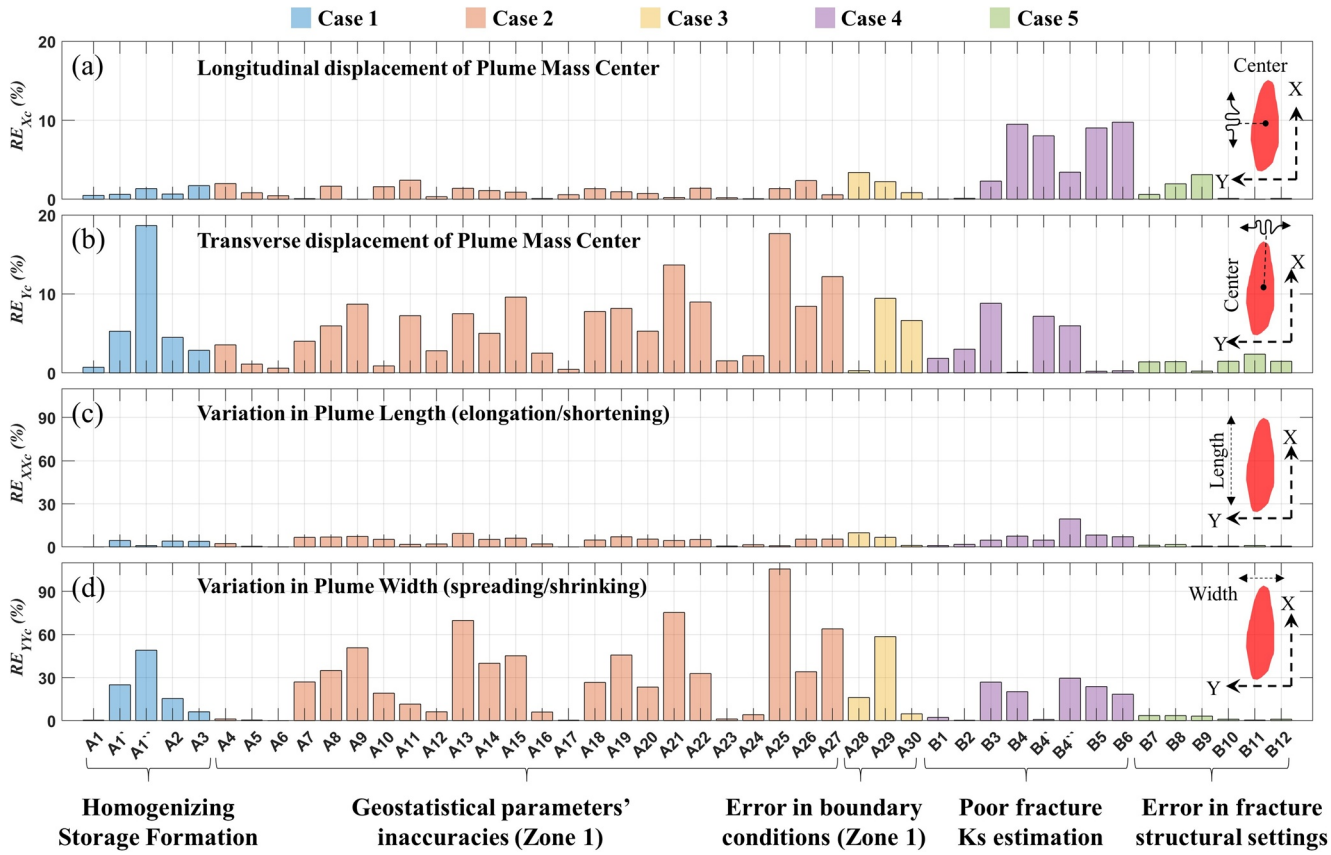

Figure 6. (a and b) The resultant relative errors (RE) in the location of the plume center and (c and d) plume width categorized by the five studied uncertainty cases. The graph includes a cartoon illustrating what is meant under each type of RE and the coordinates adapted in the estimation of the RE (Figure 5). The *y*-axis changes dramatically from (a and b) to (c and d).

(Figure 5b) and used to address the impact of these equivalent assumptions in additional scenarios (A1′, A1″, B4′, and B4″). The adapted heterogeneity realizations of Zone 1 in the uncertainty scenarios from A4 to A27 can be found in Figure S5.

4.3. Relative Error Analysis of the Numerical Experiments

The following discussion is divided into five primary subsections, each addressing a different practical case of uncertainty and its respective scenarios (Table 3). The errors in plume predictions associated with all 46 scenarios are presented in Figure 6. When viewed collectively, the results showed significantly lower relative errors (REs) in the longitudinal position of the predicted plume center and spread (*X*c and *XX*c) compared to the REs in its transverse location and spread (*Y*c and *YY*c), except scenarios B3–B6. Therefore, in the following discussion a particular focus will be given to the REs in plume transverse center and spread (RE_{Yc} and RE_{YYc}), and to the RE_{Xc} for scenarios B3–B6 only. It should be noted that errors in predicting the transverse position and spread of the plume are more critical for identifying the likely impacted areas in the shallow zone, as the errors in the longitudinal direction are more related to the plume arrival times.

4.3.1. Assuming Homogeneous Storage Formation (Case 1)

Under most standard field operations, only low-resolution data regarding the storage reservoir are readily available. Modelers, therefore, often represent the heterogeneous storage zone with an equivalent (homogeneous) *K* value (e.g., Class et al., 2009; Keating, Newell, et al., 2013; Vermeul et al., 2016). In this context, Scenarios A1–A3 investigated how the accuracy of the estimated equivalent *K* for the heterogeneous storage zone can impact the simulation results. Except for Scenario A2, these scenarios showed a reasonable prediction of the plume transverse position and spread ($RE_{Yc} < 4.5\%$ and $RE_{YYc} < 6.5\%$). Scenario A2 resulted in

a relatively high error in the plume width (RE_{YYc} = 15.4%) due to a reduction in the leakage flux caused by the low equivalent *K* assigned in Zone 1. Such lowered leakage flux allowed the transverse flow in Zone 2 to enhance plume spreading. The reasonable prediction of the plume migration in Scenario A1 can be due to the homogeneously packed part in Zone 1 that made the inflow to the fractures uniform.

Unlike Scenario A1, the impact of homogenizing a fully heterogeneous storage formation was evaluated through Scenarios A1′ and A1″. Using an equivalent *K* under those scenarios resulted in the largest RE in plume transverse position among all tested scenarios (19%) and caused a RE in plume spread up to 49%. It was noted that the main cause of these errors is the inaccurate representation of the permeability field underling the fractures by homogenizing the entire storage zone. Therefore, the homogeneity assumption for the storage formation should only be considered when the layer underling the damage zone is homogeneous, and the equivalent *K* is representative for this layer. Therefore, it is important to first identify the potential leakage pathways in the Caprock (Ingram & Urai, 1999; Ligtenberg, 2005) and then characterize the local heterogeneity underling them with high-resolution methods, such as cross-well seismic imaging (Nalonnil & Marion, 2012; Yu et al., 2008).

4.3.2. Storage Formation Geostatistical Parameter Uncertainties (Case 2)

The availability of high-resolution data to accurately estimate the geostatistical parameters of the storage formation heterogeneity is typically rare. This raises a question of what our prediction accuracy would be if such data were available. In order to explore this case, different realizations of ln*K* distribution were considered in Scenarios A4–A6 while maintaining the geostatistics of the storage zone heterogeneity in the original reference scenario. Results of these simulations revealed a RE in the plume size and the transverse location of the plume center less than 3.5% and 1.2%, respectively. This suggests that knowing the actual K distribution relative to fracture locations is still important for obtaining acutely accurate plume predictions.

Scenarios A4–A6 exhibited less REs than of those calculated under scenarios incorporating geostatistical parameter uncertainty (A7–A27). Results from these scenarios showed that inaccurate estimate of the mean ln*K* ($\mu_{\ln K}$) can lead to a significant error in the predicted brine leakage compared to the ln*K* variance ($\sigma^2_{\ln K}$) or the correlation length (λ_L). The error in the predicted transverse location of plume center (RE_{Yc}) was shown to increase by 4%–17% when $\mu_{\ln K}$ was decreased from 3.8 to 2.5. Lowering the $\mu_{\ln K}$ of Zone 1 decreased the leakage flux through the fractures and across Zone 2. This allowed Zone 2 transverse flow to control the plume position and cause a large spreading of the mass (average RE_{YYc} = 51%) compared to scenarios with correct $\mu_{\ln K}$ (average RE_{YYc} = 9%). Uncertainty in $\sigma^2_{\ln K}$ or λ_L (Scenarios A10–A12, A16–A18, and A22–A24) yielded moderate to high RE_{Yc} values (~0.4%–9%). Therefore, the $\mu_{\ln K}$ of the storage formation should be well estimated and defined in the model even if some uncertainty is expected in our estimates of the ln*K* distribution variance and correlation lengths.

The largest REs in the predicted plume position and size under Case 2 were observed in Scenarios A21, A25, and A27. In these scenarios, the plume center was largely deviated ($RE_{Yc} \approx$ 12%–17%) as a result of the presence of low *K* inclusions blocking fracture numbers 3–6 (Figure S5), which reduced the overall leakage flux and affected the hydraulic head distribution at the source. Under this head distribution, the plume migrated along different pathway from the leakage source. A larger spreading of the plume (RE_{YYc} between 63% and 105%) was also observed in these scenarios because the transverse flow in Zone 2 became more dominant after leakage flux was reduced. These simulations emphasize again the importance of local heterogeneity characterization discussed in Case 1.

4.3.3. Uncertainty in Storage Formation Boundary Conditions (Case 3)

Accurately evaluating the hydraulic head in a storage formation can be challenging in the field. In Scenarios A28–A30, a 2% error was assumed in the constant head BCs of Zone 1 to mimic limitations of field measurements. Results showed that the plume width and its transverse position were more sensitive to lowering the downstream head (BC2) than increasing the upstream head (BC1) in Zone 1. Increasing BC1 by 2% resulted in a RE_{Yc} of 0.3% and a RE_{YYc} of 16%, while decreasing BC2 by 2% resulted in a RE_{Yc} of 9.5% and a RE_{YYc} of 59%. Lowering the head at BC2 (Scenario A29) redirected a significant portion of the background flow in Zone 1 toward this downstream boundary reducing the leakage flow from the fractures. Such reduction in the leakage flow allowed the transverse flow in Zone 2 to displace the plume and enhance its spreading. However, in Scenario A28, elevating the upstream head (BC1) increased the hydraulic gradient over the

entire problem domain (between Zones 1 and 3). Therefore, the longitudinal flow in Zone 2 was increased, which limited the impact of the transverse flow of this zone on the plume.

By including both errors in Zone 1 BCs (Scenario A30), opposing effects were promoted on the leakage flow, which maintained the plume velocity in Zone 2 and limited the error in its spread. However, under this scenario the RE in the plume transverse position was relatively high (RE_{Yc} ~6%) due to the induced changes in the head distribution at the source by the inaccurate BCs. This suggests that both BCs of the storage formation, particularly the downstream one, should be accurately defined in the model to make reasonable predictions.

4.3.4. Uncertainty in Fracture Hydraulic Conductivities (Case 4)

In Scenarios B1 and B2, the hydraulic conductivities of the fractures (K_{fracs}) were multiplied by factors of 2 and 0.5, respectively, to investigate the impact of this parameter on model results. These scenarios resulted in small REs in plume transverse position and spread ($RE_{Yc} < 3.0$ and $RE_{YYc} < 2.2$). However, in Scenario B3, where accurate K_{fracs} were estimated at false locations in the caprock (i.e., reversing the order of the six K_{fracs} while maintaining the fracture locations), RE_{Yc} and RE_{YYc} were up to 8.8% and 27%, respectively. This highlights that the spatial distribution of the inferred fracture hydraulic conductivities can be more important than their magnitudes.

By assuming an equivalent single leakage pathway (Scenario B4), the RE in plume position was significantly lower than in plume spread ($RE_{Yc} = 0.1\%$ and $RE_{YYc} = 20\%$). Notably that by adding a margin of error to the used equivalent K of this single pathway (Scenarios B5 and B6), the REs almost did not change, which again shows the low sensitivity of model predictions to the magnitude of K_{fracs}. In addition, comparing Scenarios B3 and B4 shows that assuming a single leakage pathway to represent discrete fractures can result in more accurate predictions than assigning wrong distribution of the fracture permeabilities.

The above resulted low RE in the plume transverse position when a single leakage pathway was assumed (Scenario B4) can be attributed to the effect of streamlining the inflow to the fractures by the packed homogeneous part in Zone 1. However, when a fully heterogeneous storage formation was considered (Scenarios B4′ and B4″), assuming a single leakage pathway resulted in a reasonably high RE in plume transverse position and spread (max $RE_{Yc} = 7\%$ and max $RE_{YYc} = 29.5\%$). It should be noted that the maximum RE in the predicted plume transverse position under these scenarios was still less than Scenario B3, where the inferred K_{fracs} were assigned wrongly to the accurately identified fracture locations in the caprock.

Only Scenarios B3–B6 showed a noticeable error in the longitudinal location of the plume mass center (RE_{Xc} ranged between 4.8% and 15.5%). This can be explained by the augmented focused leakage flow through the assumed single pathway. Therefore, assuming a single leakage pathway can affect the prediction of the plume arrival times.

4.3.5. Poor Characterization of Fracture Structural Settings (Case 5)

As shown in Figure 6, the impact of altering the fracture structural settings slightly was minor on the prediction plume pathway and spread. This can be due to two reasons; (a) the homogeneously packed part in Zone 1 and (b) the limited variation in the fracture sizes and locations in the tested scenarios (Table 3) because of the relatively short transverse length-scale of the soil tank (123 cm). Given the findings of Hyman et al. (2020), discussed in the introduction, it is recommended to further explore the impact of uncertainty in fracture network structure on brine migration using a larger scale problem domain.

5. Summary and Conclusion

Predicting brine leakage pathways is essential to assess the contamination risk to USDW overlaying deep saline formations used in CO_2 geologic sequestration. Due to the difficulty of characterizing leakage source conditions with high accuracy in the field, model predictions of these potential leakage pathways can have a significant margin of uncertainty. Analysis presented herein based on intermediate-scale testing and numerical experiments allowed to draw the following conclusions that will enhance the practice of modeling brine leakage in CGS operations:

1. The calibrated flow and transport model developed using FEFLOW, a conventional ADE-based code, was validated to simulate the process of brine migration through a multilayered heterogeneous aquifer system represented in an intermediate-scale laboratory tank that simulated the interacting regional natural and leakage flows.
2. The analysis conducted in this study, using an intermediate-scale tank setting, showed that the lack of accurate representation of the storage zone heterogeneity can cause errors up to 19% in the predicted plume pathway and 100% in its spread. The significance of this uncertainty impact will vary depending on the real field conditions, but it can be concluded that heterogeneity of the deep storage zone, particularly in the vicinity of the potential caprock damage zone, should be well defined in the model for making reasonable predictions of brine leakage plume.
3. Plume prediction is highly sensitive to the mean value of the hydraulic conductivity (K) field of the storage zone compared to the other geostatistical parameters defining K distribution (variance and correlation lengths); uncertainty in the mean K can elevate the error in the predicted plume pathway by 17%.
4. High-resolution characterization of the storage zone permeability field can be challenging. Therefore, using an equivalent (homogeneous) K value in the simulations has been often applied. The scenario analysis conducted showed that homogeneity assumption in the vicinity of the leakage fracture produces errors up to 19% and 49% in the plume pathway and spread, respectively. These findings highlight the importance of accurately characterizing the local heterogeneity underneath the potential fracture zones instead of mapping the entire permeability field of the storage formation.
5. The leakage pathway in the caprock may not be a single fracture but a damaged zone through which brine escapes to the overlying formations. Due to prohibiting investigation costs, modelers represent the damage zone by a single equivalent leakage pathway. The analysis showed that not representing the leakage zone as an equivalent leakage pathway can result in slightly less errors compared to assigning inaccurate discrete fracture permeabilities. However, both cases revealed an error around 8% in the predicted plume pathway, which will vary depending on site conditions.
6. When a leakage event occurs due to the sudden opening of a fracture, the vertical pressure gradients resulting from the high confining pressure in the storage zone will produce a vertical flow. In the deep overlaying formations located close to the fractures, the flow velocities are expected to be high. As the leakage driven-flow travels upward, it interacts with the regional natural flow field. The analysis showed that prescribing the lateral (or regional) flow field is essential for the prediction of the plume pathway and spread at the entry of the shallow aquifers.
7. In the simulations, it is necessary to define the boundary conditions in the storage formation as accurately as possible to predict the flow field contributing to the development of the brine plume. The analysis showed that a small error in the storage zone boundary conditions (around 2%), particularly the downstream one, can significantly affect the accuracy of plume prediction (error up to 9.5% and 59% in the plume pathway and spread). This finding suggests the importance of obtaining data to define the storage zone boundary conditions during site characterization.

Above findings pointed out which of the characterization parameters result in the largest errors in the predictions. This knowledge will help to cost-efficiently investigate source conditions and thus improve site selection and design of CGS operations. This is particularly critical for cases where the storage zone caprock is overlaid by USDWs and can potentially leak under high injection stresses. The results also highlight that risk assessment studies developed based on poor characterization of source conditions can be misleading and unreliable. Thus, CGS stakeholders, such as local communities, industry, government, NGOs, and society (Johnsson et al., 2010; Setiawan & Cuppen, 2013), can evaluate the accuracy of identified areas and activities to be impacted by a CGS operation in a risk assessment study using above findings.

It is important to note that in the interpretation of the results from this laboratory-based study, the quantification of uncertainties is not directly applicable to different field settings that may be encountered at potential CGS sites. Applying the intermediate-scale testing approach gave us the opportunity to assess the impact of uncertainty under a full knowledge of the system heterogeneity and physical processes controlling the leakage at the source, which is not possible in the field. Therefore, the study was able to provide important insights for modeling field scale problems. In addition, findings of this study could be extended to shed light on possible errors in predicting CO_2 leakage, other gas migration problems, and brine leakage in other deep injection applications like hydraulic fracturing and deep waste disposal.

Data Availability Statement

Raw data generated during the experiments of the present study are publicly available and stored in the HydroShare digital repository https://doi.org/10.4211/hs.557dc959947842eb8aaf5d5427a21be3.

Acknowledgments
The authors gratefully acknowledge funding from the NSF Hydrologic Sciences Program Award 1702060. In addition, we also acknowledge the Inter-Excellence Grant No. LTAUSA19021 of the Ministry of Education, Youth and Sports of the Czech Republic that supported Jakub Solovský to participate in this project. Authors would like to express their appreciation to DHI, USA for supporting this research by offering an academic license of FEFLOW. We greatly thank all graduate and undergrad students who helped during the experimental work of this study: Jordan Skipwith, Forrest Pilone, Joon Moon, William Konishi, Anouk Uragoda, Analise Butler, and Gianna Pittman. In addition, J. Stults, S. Shea, and A. Maizel provided fruitful discussions and feedbacks.

References

Agartan, E. (2015). *Fundamental study on the effects of heterogeneity on trapping of dissolved CO_2 in deep geological formations through intermediate-scale testing and numerical modeling* (PhD dissertation). Colorado School of Mines.

Andreani, M., Gouze, P., Luquot, L., & Jouanna, P. (2008). Changes in seal capacity of fractured claystone caprocks induced by dissolved and gaseous CO_2 seepage. *Geophysical Research Letters*, *35*(14), L14404. https://doi.org/10.1029/2008gl034467

Bachu, S. (2003). Screening and ranking of sedimentary basins for sequestration of CO_2 in geological media in response to climate change. *Environmental Geology*, *44*(3), 277–289. https://doi.org/10.1007/s00254-003-0762-9

Bandilla, K. W., Celia, M. A., Birkholzer, J. T., Cihan, A., & Leister, E. C. (2015). Multiphase modeling of geologic carbon sequestration in saline aquifers. *Groundwater*, *53*(3), 362–377. https://doi.org/10.1111/gwat.12315

Barth, G. R., Hill, M. C., Illangasekare, T. H., & Rajaram, H. (2001). Predictive modeling of flow and transport in a two-dimensional intermediate-scale, heterogeneous porous medium. *Water Resources Research*, *37*(10), 2503–2512. https://doi.org/10.1029/2001wr000242

Barth, G. R., Illangasekare, T. H., Hill, M. C., & Rajaram, H. (2001). A new tracer-density criterion for heterogeneous porous media. *Water Resources Research*, *37*(1), 21–31. https://doi.org/10.1029/2000wr900287

Benson, D. A., Wheatcraft, S. W., & Meerschaert, M. M. (2000a). Application of a fractional advection-dispersion equation. *Water Resources Research*, *36*(6), 1403–1412. https://doi.org/10.1029/2000wr900031

Benson, D. A., Wheatcraft, S. W., & Meerschaert, M. M. (2000b). The fractional-order governing equation of Lévy motion. *Water Resources Research*, *36*(6), 1413–1423. https://doi.org/10.1029/2000wr900032

Bird, R. B., Stewart, W. E., & Lightfoot, E. N. (1960). *Transport phenomena*. New York: John Wiley & Sons.

Birkholzer, J. T., Nicot, J. P., Oldenburg, C. M., Zhou, Q., Kraemer, S., & Bandilla, K. (2011). Brine flow up a well caused by pressure perturbation from geologic carbon sequestration: Static and dynamic evaluations. *International Journal of Greenhouse Gas Control*, *5*(4), 850–861. https://doi.org/10.1016/j.ijggc.2011.01.003

Birkholzer, J. T., & Zhou, Q. (2009). Basin-scale hydrogeologic impacts of CO_2 storage: Capacity and regulatory implications. *International Journal of Greenhouse Gas Control*, *3*(6), 745–756. https://doi.org/10.1016/j.ijggc.2009.07.002

Birkholzer, J. T., Zhou, Q., & Tsang, C. F. (2009). Large-scale impact of CO_2 storage in deep saline aquifers: A sensitivity study on pressure response in stratified systems. *International Journal of Greenhouse Gas Control*, *3*(2), 181–194. https://doi.org/10.1016/j.ijggc.2008.08.002

Bixler, N. E. (1989). An improved time integrator for finite element analysis. *Communications in Applied Numerical Methods*, *5*(2), 69–78. https://doi.org/10.1002/cnm.1630050203

Bricker, S. H., Barkwith, A. K. A. P., MacDonald, A. M., Hughes, A. G., & Smith, M. (2012). Effects of CO_2 injection on shallow groundwater resources: A hypothetical case study in the Sherwood Sandstone aquifer, UK. *International Journal of Greenhouse Gas Control*, *11*, 337–348. https://doi.org/10.1016/j.ijggc.2012.09.001

Cavanagh, A., & Wildgust, N. (2011). Pressurization and brine displacement issues for deep saline formation CO_2 storage. *Energy Procedia*, *4*, 4814–4821. https://doi.org/10.1016/j.egypro.2011.02.447

Celia, M. A., Nordbotten, J. M., Court, B., Dobossy, M., & Bachu, S. (2011). Field-scale application of a semi-analytical model for estimation of CO_2 and brine leakage along old wells. *International Journal of Greenhouse Gas Control*, *5*(2), 257–269. https://doi.org/10.1016/j.ijggc.2010.10.005

Christison, T., Tanner, C., Madden, J. E., & Lopez, L. (2016). *Anion determinations in municipal drinking water samples using EPA method 300.1 (A) on an integrated IC system*. Sunnyvale, CA: Thermo Fisher Scientific.

Cihan, A., Birkholzer, J. T., & Bianchi, M. (2015). Optimal well placement and brine extraction for pressure management during CO_2 sequestration. *International Journal of Greenhouse Gas Control*, *42*, 175–187. https://doi.org/10.1016/j.ijggc.2015.07.025

Cihan, A., Birkholzer, J. T., & Zhou, Q. (2013). Pressure buildup and brine migration during CO_2 storage in multilayered aquifers. *Groundwater*, *51*(2), 252–267.

Class, H., Ebigbo, A., Helmig, R., Dahle, H. K., Nordbotten, J. M., Celia, M. A., et al. (2009). A benchmark study on problems related to CO_2 storage in geologic formation. *Computational Geosciences*, *14*(1), 409. https://doi.org/10.1007/s10596-009-9146-x

Cohen, H. A., Parratt, T., & Andrews, C. B. (2013). Potential contaminant pathways from hydraulically fractured shale to aquifers. *Groundwater*, *51*(3), 317–319.

Darcy, H. P. G. (1856). *Les Fontaines publiques de la ville de Dijon. Exposition et application des principes à suivre et des formules à employer dans les questions de distribution d'eau*. Paris: V. Dalamont.

Delfs, J. O., Nordbeck, J., & Bauer, S. (2016). Upward brine migration resulting from pressure increases in a layered subsurface system. *Environmental Earth Sciences*, *75*(22), 1441. https://doi.org/10.1007/s12665-016-6245-6

Detwiler, R. L., & Morris, J. P. (2019). Fracture initiation, propagation, and permeability evolution. In: In S. Vialle, J. Ajo-Franklin, J. William Carey (Eds.), *Geological carbon storage: Subsurface seals and caprock integrity. Geophysical Monograph Series* (pp. 121–135). American Geophysical Union by John Wiley & Sons.

Deutsch, C. V. (1998). Fortran programs for calculating connectivity of three-dimensional numerical models and for ranking multiple realizations. *Computers & Geosciences*, *24*(1), 69–76. https://doi.org/10.1016/s0098-3004(97)00085-x

Diersch, G. H. J. (2014). FEFLOW: Finite element modeling of flow, mass and heat transport in porous and fractured media (Vol. 10, pp. 978–983). Heidelberg: Springer Science + Business Media.

Doherty, J. E. (1994). *PEST: A unique computer program for model-independent parameter optimisation. Water down under 94: Groundwater/surface hydrology common interest papers; preprints of papers* (No. 94/10, pp. 551–554). Barton, ACT,Australia: Institution of Engineers; National Conference Publication.

Doherty, J. E. (2015). *Calibration and uncertainty analysis for complex environmental models. Watermark numerical computing* (1st ed.). Brisbane, Australia: Watermark Numerical Computing.

Doherty, J. E., Hunt, R. J., & Tonkin, M. J. (2010). *Approaches to highly parameterized inversion: A guide to using PEST for model-parameter and predictive-uncertainty analysis*. (Scientific Investigations Report No. 2010-5211, p. 71). US Geological Survey. https://doi.org/10.3133/sir20105211

Doughty, C., Freifeld, B. M., & Trautz, R. C. (2008). Site characterization for CO_2 geologic storage and vice versa: The Frio brine pilot, Texas, USA as a case study. *Environmental Geology*, *54*(8), 1635–1656. https://doi.org/10.1007/s00254-007-0942-0

Farrell, D. A., Woodbury, A. D., & Sudicky, E. A. (1994). The 1978 Borden tracer experiment: Analysis of the spatial moments. *Water Resources Research*, *30*(11), 3213–3223. https://doi.org/10.1029/94wr00622

Fetter, C. W., Boving, T., & Kreamer, D. (2017). *Contaminant hydrogeology* (3rd ed.). Long Grove: Waveland Press.

Freyberg, D. L. (1986). A natural gradient experiment on solute transport in a sand aquifer: 2. Spatial moments and the advection and dispersion of nonreactive tracers. *Water Resources Research*, *22*(13), 2031–2046. https://doi.org/10.1029/wr022i013p02031

Garabedian, S. P., LeBlanc, D. R., Gelhar, L. W., & Celia, M. A. (1991). Large-scale natural gradient tracer test in sand and gravel, Cape Cod, Massachusetts: 2. Analysis of spatial moments for a nonreactive tracer. *Water Resources Research*, *27*(5), 911–924. https://doi.org/10.1029/91wr00242

Gasda, S. E., Bachu, S., & Celia, M. A. (2004). Spatial characterization of the location of potentially leaky wells penetrating a geological formation in a mature sedimentary basin. *Environmental Geology*, *46*(6–7), 707–720. https://doi.org/10.1007/s00254-004-1073-5

Gelhar, L. W., Welty, C., & Rehfeldt, K. R. (1992). A critical review of data on field-scale dispersion in aquifers. *Water Resources Research*, *28*(7), 1955–1974. https://doi.org/10.1029/92wr00607

Gresho, P. M., Lee, R. L., Sani, R. L., & Stullich, T. W. (1979). *Time-dependent FEM solution of the incompressible Navier-Stokes equations in two-and three-dimensions* (Preprint UCRL-81323). Lawrence Livermore National Laboratory, California University.

Gupta, P. K., & Yadav, B. (2020). Leakage of CO_2 from geological storage and its impacts on fresh soil–water systems: A review. *Environmental Science and Pollution Research*, *27*(12), 12995–13018. https://doi.org/10.1007/s11356-020-08203-7

Hautman, D. P., & Munch, D. J. (1997). *Method 300.1 determination of inorganic anions in drinking water by ion chromatography*. Cincinnati, OH: U.S. Environmental Protection Agency.

Hermanrud, C., Andresen, T., Eiken, O., Hansen, H., Janbu, A., Lippard, J., et al. (2009). Storage of CO_2 in saline aquifers–lessons learned from 10 years of injection into the Utsira Formation in the Sleipner area. *Energy Procedia*, *1*(1), 1997–2004. https://doi.org/10.1016/j.egypro.2009.01.260

Hess, K. M., Wolf, S. H., & Celia, M. A. (1992). Large-scale natural gradient tracer test in sand and gravel, Cape Cod, Massachusetts: 3. Hydraulic conductivity variability and calculated macrodispersivities. *Water Resources Research*, *28*(8), 2011–2027. https://doi.org/10.1029/92wr00668

Hunt, R. J., Luchette, J., Schreuder, W. A., Rumbaugh, J. O., Doherty, J., Tonkin, M. J., & Rumbaugh, D. B. (2010). Using a cloud to replenish parched groundwater modeling efforts. *Groundwater*, *48*(3), 360–365. https://doi.org/10.1111/j.1745-6584.2010.00699.x

Hyman, J. D., Jimenez-Martinez, J., Gable, C. W., Stauffer, P. H., & Pawar, R. J. (2020). Characterizing the impact of fractured caprock heterogeneity on supercritical CO_2 injection. *Transport in Porous Media*, *131*(3), 935–955. https://doi.org/10.1007/s11242-019-01372-1

Ingram, G. M., & Urai, J. L. (1999). Top-seal leakage through faults and fractures: The role of mudrock properties. *Geological Society, London, Special Publications*, *158*, 125–135. https://doi.org/10.1144/gsl.sp.1999.158.01.10

Intergovernmental Panel on Climate Change. (2005) *IPCC special report on carbon dioxide capture and storage. Prepared by working group III of the Intergovernmental Panel on Climate Change* [In B. Metz, O. Davidson, H. C. de Coninck, M. Loos, & L. A. Meyer (Eds.)] (p. 442). Cambridge; New York: Intergovernmental Panel on Climate Change.

Jacobs, M. (2009).*A multidisciplinary approach to site characterization and remediation of contamination from oilfield-produced waters, East Poplar Oil Field, Fort Peck Indian Reservation, Roosevelt County, Montana*. San Antonio, TX SPE Americas E&P Environmental and safety Conference.

Jeanne, P., Guglielmi, Y., & Cappa, F. (2013). Dissimilar properties within a carbonate-reservoir's small fault zone, and their impact on the pressurization and leakage associated with CO_2 injection. *Journal of Structural Geology*, *47*, 25–35. https://doi.org/10.1016/j.jsg.2012.10.010

Jiang, X. (2011). A review of physical modelling and numerical simulation of long-term geological storage of CO_2. *Applied energy*, *88*(1), 3557–3566. https://doi.org/10.1016/j.apenergy.2011.05.004

Jiao, J., Zhang, Y., & Wang, L. (2019). A new inverse method for contaminant source identification under unknown solute transport boundary conditions. *Journal of Hydrology*, *577*, 123911. https://doi.org/10.1016/j.jhydrol.2019.123911

Johnsson, F., Reiner, D., Itaoka, K., & Herzog, H. (2010). Stakeholder attitudes on carbon capture and storage—An international comparison. *International Journal of Greenhouse Gas Control*, *4*(2), 410–418. https://doi.org/10.1016/j.ijggc.2009.09.006

Jones, D. G., Beaubien, S. E., Blackford, J. C., Foekema, E. M., Lions, J., De Vittor, C., et al. (2015). Developments since 2005 in understanding potential environmental impacts of CO_2 leakage from geological storage. *International Journal of Greenhouse Gas Control*, *40*, 350–377. https://doi.org/10.1016/j.ijggc.2015.05.032

Keating, E. H., Fessenden, J., Kanjorski, N., Koning, D. J., & Pawar, R. (2010). The impact of CO_2 on shallow groundwater chemistry: Observations at a natural analog site and implications for carbon sequestration. *Environmental Earth Sciences*, *60*(3), 521–536. https://doi.org/10.1007/s12665-009-0192-4

Keating, E. H., Hakala, J. A., Viswanathan, H., Carey, J. W., Pawar, R., Guthrie, G. D., & Fessenden-Rahn, J. (2013). CO_2 leakage impacts on shallow groundwater: Field-scale reactive-transport simulations informed by observations at a natural analog site. *Applied Geochemistry*, *30*, 136–147. https://doi.org/10.1016/j.apgeochem.2012.08.007

Keating, E. H., Newell, D. L., Dempsey, D., & Pawar, R. (2014). Insights into interconnections between the shallow and deep systems from a natural CO_2 reservoir near Springerville, Arizona. *International Journal of Greenhouse Gas Control*, *25*, 162–172. https://doi.org/10.1016/j.ijggc.2014.03.009

Keating, E. H., Newell, D. L., Viswanathan, H., Carey, J. W., Zyvoloski, G., & Pawar, R. (2013b). CO_2/brine transport into shallow aquifers along fault zones. *Environmental Science & Technology*, *47*(1), 290–297. https://doi.org/10.1021/es301495x

Kharaka, Y. K., Cole, D. R., Thordsen, J. J., Gans, K. D., & Thomas, R. B. (2013). Geochemical monitoring for potential environmental impacts of geologic sequestration of CO_2. *Reviews in Mineralogy and Geochemistry*, *77*(1), 399–430. https://doi.org/10.2138/rmg.2013.77.11

Kharaka, Y. K., Cole, D. R., Thordsen, J. J., Kakouros, E., & Nance, H. S. (2006). Gas–water–rock interactions in sedimentary basins: CO_2 sequestration in the Frio Formation, Texas, USA. *Journal of Geochemical Exploration*, *89*(1–3), 183–186. https://doi.org/10.1016/j.gexplo.2005.11.077

Kharaka, Y. K., Thordsen, J. J., Hovorka, S. D., Nance, H. S., Cole, D. R., Phelps, T. J., & Knauss, K. G. (2009). Potential environmental issues of CO_2 storage in deep saline aquifers: Geochemical results from the Frio-I Brine Pilot test, Texas, USA. *Applied Geochemistry*, *24*(6), 1106–1112. https://doi.org/10.1016/j.apgeochem.2009.02.010

Kissinger, A., Noack, V., Knopf, S., Konrad, W., Scheer, D., & Class, H. (2017). Regional-scale brine migration along vertical pathways due to CO_2 injection–Part 2: A simulated case study in the North German Basin. *Hydrology and Earth System Sciences*, *21*(6), 2751–2775. https://doi.org/10.5194/hess-21-2751-2017

Lackner, K. S. (2003). A guide to CO_2 sequestration. *Science*, *300*(5626), 1677–1678. https://doi.org/10.1126/science.1079033
Lei, Q., Latham, J. P., & Tsang, C. F. (2017). The use of discrete fracture networks for modelling coupled geomechanical and hydrological behaviour of fractured rocks. *Computers and Geotechnics*, *85*, 151–176. https://doi.org/10.1016/j.compgeo.2016.12.024
Lenhard, R. J., Oostrom, M., Simmons, C. S., & White, M. D. (1995). Investigation of density-dependent gas advection of trichloroethylene: Experiment and a model validation exercise. *Journal of Contaminant Hydrology*, *19*(1), 47–67. https://doi.org/10.1016/0169-7722(94)00055-m
Li, Q., & Liu, G. (2016). Risk assessment of the geological storage of CO_2: A review. In: In V. Vishal & T. N. Singh (Eds.), *Geologic carbon sequestration*. (pp. 249–284). Springer. https://doi.org/10.1007/978-3-319-27019-7_13
Ligtenberg, J. H. (2005). Detection of fluid migration pathways in seismic data: Implications for fault seal analysis. *Basin Research*, *17*(1), 141–153. https://doi.org/10.1111/j.1365-2117.2005.00258.x
Lions, J., Devau, N., de Lary, L., Dupraz, S., Parmentier, M., Gombert, P., & Dictor, M. C. (2014). Potential impacts of leakage from CO_2 geological storage on geochemical processes controlling fresh groundwater quality: A review. *International Journal of Greenhouse Gas Control*, *22*, 165–175. https://doi.org/10.1016/j.ijggc.2013.12.019
Llewellyn, G. T. (2014). Evidence and mechanisms for Appalachian Basin brine migration into shallow aquifers in NE Pennsylvania, USA. *Hydrogeology Journal*, *22*(5), 1055–1066. https://doi.org/10.1007/s10040-014-1125-1
Luyun, R., Jr., Momii, K., & Nakagawa, K. (2011). Effects of recharge wells and flow barriers on seawater intrusion. *Groundwater*, *49*(2), 239–249. https://doi.org/10.1111/j.1745-6584.2010.00719.x
Morris, J. P., Fu, P., Settgast, R. R., Sherman, C. S., Friedrich, M., & Leonard, P. (2016). *The combined influence of stress barriers and natural fractures upon hydraulic fracture height growth*. Paper presented at the 50th US Rock Mechanics/Geomechanics Symposium. American Rock Mechanics Association.
Myers, T. (2012). Potential contaminant pathways from hydraulically fractured shale to aquifers. *Groundwater*, *50*(6), 872–882. https://doi.org/10.1111/j.1745-6584.2012.00933.x
Nalonnil, A., & Marion, B. (2012). High-resolution reservoir monitoring using crosswell seismic. *SPE Reservoir Evaluation and Engineering*, *15*(1), 25–30.
Nelson, C. R., Evans, J. M., Sorensen, J. A., Steadman, E. N., & Harju, J. A. (2005). *Factors affecting the potential for CO_2 leakage from geological sinks, Grand Forks*. NDEERC. Retrieved from www.undeerc.org/PCOR:PCORpartnership
NETL. (2017). *Best PRACTICES: Risk management and simulation for geologic storage projects, DOE/NETL-2017/1846*. Albany, OR; Anchorage, AK; Houston, TX; Morgantown, WV; Pittsburgh, PA: U.S. Department of Energy.
Neuman, S. P. (1990). Universal scaling of hydraulic conductivities and dispersivities in geologic media. *Water Resources Research*, *26*(8), 1749–1758. https://doi.org/10.1029/wr026i008p01749
Nicot, J. P. (2008). Evaluation of large-scale CO_2 storage on fresh-water sections of aquifers: An example from the Texas Gulf Coast Basin. *International Journal of Greenhouse Gas Control*, *2*(4), 582–593. https://doi.org/10.1016/j.ijggc.2008.03.004
Nowak, M., Myrttinen, A., Zimmer, M., Wiese, B., van Geldern, R., & Barth, J. A. (2013). Well-based, geochemical leakage monitoring of an aquifer immediately above a CO2 storage reservoir by stable carbon isotopes at the Ketzin pilot site, Germany. Energy Procedia, 40, 346–354. https://doi.org/10.1016/j.egypro.2013.08.040
Oostrom, M., Dane, J. H., & Wietsma, T. W. (2007). A review of multidimensional, multifluid, intermediate-scale experiments: Flow behavior, saturation imaging, and tracer detection and quantification. *Vadose Zone Journal*, *6*(3), 610–637. https://doi.org/10.2136/vzj2006.0178
Oostrom, M., Hayworth, J. S., Dane, J. H., & Güven, O. (1992). Behavior of dense aqueous phase leachate plumes in homogeneous porous media. *Water Resources Research*, *28*(8), 2123–2134. https://doi.org/10.1029/92wr00711
Pan, P. Z., Rutqvist, J., Feng, X. T., & Yan, F. (2013). Modeling of caprock discontinuous fracturing during CO_2 injection into a deep brine aquifer. *International Journal of Greenhouse Gas Control*, *19*, 559–575. https://doi.org/10.1016/j.ijggc.2013.10.016
Pawar, R. J., Bromhal, G. S., Carey, J. W., Foxall, W., Korre, A., Ringrose, P. S., et al. (2015). Recent advances in risk assessment and risk management of geologic CO_2 storage. *International Journal of Greenhouse Gas Control*, *40*, 292–311. https://doi.org/10.1016/j.ijggc.2015.06.014
Peng, S., & Brusseau, M. L. (2005). Impact of soil texture on air-water interfacial areas in unsaturated sandy porous media. *Water Resources Research*, *41*(31–8), W03021. https://doi.org/10.1029/2004wr003233
Person, M., Banerjee, A., Rupp, J., Medina, C., Lichtner, P., Gable, C., et al. (2010). Assessment of basin-scale hydrologic impacts of CO_2 sequestration, Illinois basin. *International Journal of Greenhouse Gas Control*, *4*(5), 840–854. https://doi.org/10.1016/j.ijggc.2010.04.004
Plampin, M. R., Porter, M. L., Pawar, R. J., & Illangasekare, T. H. (2017). Intermediate-scale experimental study to improve fundamental understanding of attenuation capacity for leaking CO_2 in heterogeneous shallow aquifers. *Water Resources Research*, *53*(12), 10121–10138. https://doi.org/10.1002/2016wr020142
Qafoku, N. P., Lawter, A. R., Bacon, D. H., Zheng, L., Kyle, J., & Brown, C. F. (2017). Review of the impacts of leaking CO_2 gas and brine on groundwater quality. *Earth-Science Reviews*, *169*, 69–84. https://doi.org/10.1016/j.earscirev.2017.04.010
Ramadas, M., Ojha, R., & Govindaraju, R. S. (2015). Current and future challenges in groundwater. II: Water quality modeling. *Journal of Hydrologic Engineering*, *20*(1), A4014008. https://doi.org/10.1061/(asce)he.1943-5584.0000936
Rathnaweera, T. D., Ranjith, P. G., & Perera, M. S. A. (2016). Experimental investigation of geochemical and mineralogical effects of CO_2 sequestration on flow characteristics of reservoir rock in deep saline aquifers. *Scientific Reports*, *6*(1–12), 19362. https://doi.org/10.1038/srep19362
Rehfeldt, K. R., Boggs, J. M., & Gelhar, L. W. (1992). Field study of dispersion in a heterogeneous aquifer: 3. Geostatistical analysis of hydraulic conductivity. *Water Resources Research*, *28*(12), 3309–3324. https://doi.org/10.1029/92wr01758
Remy, N., Boucher, A., & Wu, J. (2009). *Applied geostatistics with SGeMS: A user's guide*. New York: Cambridge University Press.
Réveillère, A., & Rohmer, J. (2011). Managing the risk of CO_2 leakage from deep saline aquifer reservoirs through the creation of a hydraulic barrier. *Energy Procedia*, *4*, 3187–3194. https://doi.org/10.1016/j.egypro.2011.02.234
Ross, G. D., Todd, A. C., & Tweedie, J. A. (1981). *The effect of simulated CO_2 flooding on the permeability of reservoir rocks enhanced oil recovery* (pp. 351–366). Amsterdam: Elsevier.
Rovey, C. W. II (1998). Digital simulation of the scale effect in hydraulic conductivity. *Hydrogeology Journal*, *6*(2), 216–225. https://doi.org/10.1007/s100400050146
Rutqvist, J., Birkholzer, J., Cappa, F., & Tsang, C. F. (2007). Estimating maximum sustainable injection pressure during geological sequestration of CO_2 using coupled fluid flow and geomechanical fault-slip analysis. *Energy Conversion and Management*, *48*(6), 1798–1807. https://doi.org/10.1016/j.enconman.2007.01.021

Rutqvist, J., Birkholzer, J. T., & Tsang, C. F. (2008). Coupled reservoir–geomechanical analysis of the potential for tensile and shear failure associated with CO_2 injection in multilayered reservoir–caprock systems. *International Journal of Rock Mechanics and Mining Sciences*, *45*(2), 132–143. https://doi.org/10.1016/j.ijrmms.2007.04.006

Saiers, J. E., & Barth, E. (2012). Potential contaminant pathways from hydraulically fractured shale aquifers. *Groundwater*, *50*(6), 826–828. https://doi.org/10.1111/j.1745-6584.2012.00990.x

Sakaki, T., & Illangasekare, T. H. (2007). Comparison of height-averaged and point-measured capillary pressure–saturation relations for sands using a modified Tempe cell. *Water Resources Research*, *43*(121–126), W12502. https://doi.org/10.1029/2006wr005814

Sarris, T. S., Close, M., & Abraham, P. (2018). Using solute and heat tracers for aquifer characterization in a strongly heterogeneous alluvial aquifer. *Journal of Hydrology*, *558*, 55–71. https://doi.org/10.1016/j.jhydrol.2018.01.032

Schumer, R., Benson, D. A., Meerschaert, M. M., & Wheatcraft, S. W. (2001). Eulerian derivation of the fractional advection–dispersion equation. *Journal of Contaminant Hydrology*, *48*(1–2), 69–88. https://doi.org/10.1016/s0169-7722(00)00170-4

Schumer, R., Meerschaert, M. M., & Baeumer, B. (2009). Fractional advection-dispersion equations for modeling transport at the Earth surface. *Journal of Geophysical Research*, *114*(F4), 1–15. https://doi.org/10.1029/2008jf001246

Setiawan, A. D., & Cuppen, E. (2013). Stakeholder perspectives on carbon capture and storage in Indonesia. *Energy Policy*, *61*, 1188–1199. https://doi.org/10.1016/j.enpol.2013.06.057

Solovský, J., Fučík, R., Plampin, M. R., Illangasekare, T. H., & Mikyška, J. (2020). Dimensional effects of inter-phase mass transfer on attenuation of structurally trapped gaseous carbon dioxide in shallow aquifers. *Journal of Computational Physics*, *405*, 109178. https://doi.org/10.1016/j.jcp.2019.109178

Sun, A. Y., Nicot, J. P., & Zhang, X. (2013). Optimal design of pressure-based, leakage detection monitoring networks for geologic carbon sequestration repositories. *International Journal of Greenhouse Gas Control*, *19*, 251–261. https://doi.org/10.1016/j.ijggc.2013.09.005

Sun, A. Y., Zeidouni, M., Nicot, J. P., Lu, Z., & Zhang, D. (2013). Assessing leakage detectability at geologic CO_2 sequestration sites using the probabilistic collocation method. *Advances in Water Resources*, *56*, 49–60. https://doi.org/10.1016/j.advwatres.2012.11.017

Taylor, G. I. (1953). Dispersion of soluble matter in solvent flowing slowly through a tube. *Proceedings of the Royal Society of London A: Mathematical and Physical Sciences*, *219*(1137), 186–203. https://doi.org/10.1098/rspa.1953.0139

Thamke, J. N. & Craig, S. D., (1997). Saline-water contamination in quaternary deposits and the Poplar River, East Poplar Oil Field, Northeastern Montana (Water-Resources Investigations Report 97-4000): U.S. Department of the Interior, U.S. Geological Survey.

Thamke, J. N. & Midtlyng, K. S., (2003). Ground-water quality for two areas in the Fort Peck Indian Reservation, Northeastern Montana, 1993–2000 Vol. (3, Water-Resources Investigations Report No. 4214): US Department of the Interior, US Geological Survey.

Thornton, S. F., Tobin, K., & Smith, J. W. (2013). Comparison of constant and transient-source zones on simulated contaminant plume evolution in groundwater: Implications for hydrogeological risk assessment. *Groundwater Monitoring & Remediation*, *33*(3), 78–91. https://doi.org/10.1111/gwmr.12008

Tillner, E., Kempka, T., Nakaten, B., & Kühn, M. (2013). Brine migration through fault zones: 3D numerical simulations for a prospective CO_2 storage site in Northeast Germany. *International Journal of Greenhouse Gas Control*, *19*, 689–703. https://doi.org/10.1016/j.ijggc.2013.03.012

Tillner, E., Langer, M., Kempka, T., & Kühn, M. (2016). Fault damage zone volume and initial salinity distribution determine intensity of shallow aquifer salinisation in subsurface storage. *Hydrology and Earth System Sciences*, *20*(3), 1049–1067. https://doi.org/10.5194/hess-20-1049-2016

Torp, T. A., & Gale, J. (2004). Demonstrating storage of CO_2 in geological reservoirs: The Sleipner and SACS projects. *Energy*, *29*(9–10), 1361–1369. https://doi.org/10.1016/j.energy.2004.03.104

Trevisan, L., Pini, R., Cihan, A., Birkholzer, J. T., Zhou, Q., González-Nicolás, A., & Illangasekare, T. H. (2017). Imaging and quantification of spreading and trapping of carbon dioxide in saline aquifers using meter-scale laboratory experiments. *Water Resources Research*, *53*(1), 485–502. https://doi.org/10.1002/2016wr019749

Tsang, C. F., Birkholzer, J., & Rutqvist, J. (2008). A comparative review of hydrologic issues involved in geologic storage of CO_2 and injection disposal of liquid waste. *Environmental Geology*, *54*(8), 1723–1737. https://doi.org/10.1007/s00254-007-0949-6

U.S. DOE. (2015). Carbon sequestration atlas of the United States and Canada (5th ed., Vol. 24). Department of Energy/NETL.

U.S. EPA. (2010). *40 CFR Parts 124, 144, 145, 146, and 147 Federal requirements under the underground injection (UIC) program for carbon dioxide (CO_2) geologic sequestration (GS) wells; Final Rule, [EPA–HQ–OW–2008–0390 FRL–9232–7], RIN 2040–AE98* (pp. 77230–77303). Washington, DC: U.S. Environmental Protection Agency.

U.S. EPA. (2016). *Definition and procedure for the determination of the method detection limit*, Revision 2. Washington, DC: U.S. Environmental Protection Agency.

Van der Meer, L. G. H. (1992). Investigations regarding the storage of carbon dioxide in aquifers in the Netherlands. *Energy Conversion and Management, 33*(5–8), 611–618. https://doi.org/10.1016/0196-8904(92)90063-3

Vermeul, V. R., Amonette, J. E., Strickland, C. E., Williams, M. D., & Bonneville, A. (2016). An overview of the monitoring program design for the FutureGen 2.0 CO_2 storage site. *International Journal of Greenhouse Gas Control*, *51*, 193–206. https://doi.org/10.1016/j.ijggc.2016.05.023

Vialle, S., Druhan, J. L., & Maher, K. (2016). Multi-phase flow simulation of CO_2 leakage through a fractured caprock in response to mitigation strategies. *International Journal of Greenhouse Gas Control*, *44*, 11–25. https://doi.org/10.1016/j.ijggc.2015.10.007

Wainwright, H. M., Finsterle, S., Zhou, Q., & Birkholzer, J. T. (2013). Modeling the performance of large-scale CO_2 storage systems: A comparison of different sensitivity analysis methods. *International Journal of Greenhouse Gas Control*, *17*, 189–205. https://doi.org/10.1016/j.ijggc.2013.05.007

Willmann, M., Carrera, J., & Sánchez-Vila, X. (2008). Transport upscaling in heterogeneous aquifers: What physical parameters control memory functions? *Water Resources Research*, *44*(12), W12437. https://doi.org/10.1029/2007wr006531

Wunsch, A., Navarre-Sitchler, A. K., & McCray, J. E. (2013). Geochemical implications of brine leakage into freshwater aquifers. *Groundwater*, *51*(6), 855–865. https://doi.org/10.1111/gwat.12011

Xie, J., Zhang, K., Hu, L., Pavelic, P., Wang, Y., & Chen, M. (2015). Field-based simulation of a demonstration site for carbon dioxide sequestration in low-permeability saline aquifers in the Ordos Basin, China. *Hydrogeology Journal*, *23*(7), 1465–1480. https://doi.org/10.1007/s10040-015-1267-9

Xie, J., Zhang, K., Hu, L., Wang, Y., & Chen, M. (2015). Understanding the carbon dioxide sequestration in low-permeability saline aquifers in the Ordos Basin with numerical simulations. *Greenhouse Gases: Science and Technology*, *5*(5), 558–576. https://doi.org/10.1002/ghg.1499

Yamamoto, H., Zhang, K., Karasaki, K., Marui, A., Uehara, H., & Nishikawa, N., (2009). Numerical investigation concerning the impact of CO_2 geologic storage on regional groundwater flow. *International Journal of Greenhouse Gas Control*, *3*(5), 586–599. https://doi.org/10.1016/j.ijggc.2009.04.007

Yoon, H., & McKenna, S. A., (2012). Highly parameterized inverse estimation of hydraulic conductivity and porosity in a three-dimensional, heterogeneous transport experiment. *Water Resources Research*, *48*(10), W10536. https://doi.org/10.1029/2012wr012149

Yu, G., Marion, B., Bryans, B., Carrillo, P., Guo, W., Pang, Y., & Kong, F. (2008). Crosswell seismic imaging for deep gas reservoir characterization. *Geophysics*, *73*(6), B117–B126. https://doi.org/10.1190/1.2980417

Zeidouni, M., Nicot, J. P., & Hovorka, S. D. (2014). Monitoring above-zone temperature variations associated with CO_2 and brine leakage from a storage aquifer. *Environmental Earth Sciences*, *75*(5), 1733–1747. https://doi.org/10.1007/s12665-014-3077-0

Zhang, Y., Benson, D. A., & Baeumer, B. (2008). Moment analysis for spatiotemporal fractional dispersion. *Water Resources Research*, *44*(4), W04424. https://doi.org/10.1029/2007wr006291

Zhang, Y., Benson, D. A., Meerschaert, M. M., & LaBolle, E. M. (2007). Space-fractional advection-dispersion equations with variable parameters: Diverse formulas, numerical solutions, and application to the macrodispersion experiment site data. *Water Resources Research*, *43*(5), W05439. https://doi.org/10.1029/2006wr004912

Zhang, Y., Benson, D. A., & Reeves, D. M. (2009). Time and space nonlocalities underlying fractional-derivative models: Distinction and literature review of field applications. *Advances in Water Resources*, *32*(4), 561–581. https://doi.org/10.1016/j.advwatres.2009.01.008

Zhang, Y., Person, M., & Merino, E. (2005). Hydrologic and geochemical controls on soluble benzene migration in sedimentary basins. *Geofluids*, *5*(2), 83–105. https://doi.org/10.1111/j.1468-8123.2005.00101.x

Zhao, R., Cheng, J., & Zhang, K. (2012). CO_2 plume evolution and pressure buildup of large-scale CO_2 injection into saline aquifers in Sanzhao Depression, Songliao Basin, China. *Transport Porous Media, 95*(2), 407–424. https://doi.org/10.1007/s11242-012-0052-7

Zheng, C., & Wang, P. P. (1999). *MT3DMS: A modular three-dimensional multispecies transport model for simulation of advection, dispersion, and chemical reactions of contaminants in groundwater systems; documentation and user's guide* (Contract Report SERDP-99-1, p. 169). Vicksburg, MS: US Army Engineer Research and Development Center.

Zhou, Q., Birkholzer, J. T., Mehnert, E., Lin, Y. F., & Zhang, K. (2010). Modeling basin-and plume-scale processes of CO_2 storage for full-scale deployment. *Groundwater*, *48*(4), pp. 494–514.

Zweigel, P., Arts, R., Lothe, A. E., & Lindeberg, E. B. (2004). Reservoir geology of the Utsira formation at the first industrial-scale underground CO_2 storage site (Sleipner area, North Sea), *Geological Society, London, Special Publications*, *233*(1), 165–180. https://doi.org/10.1144/gsl.sp.2004.233.01.11